Anti-cathepsin D immunotherapy triggers both innate and adaptive anti-tumour immunity in breast cancer

Timothée David, Aude Mallavialle, Julien Faget, Lindsay B Alcaraz, Marion Lapierre, Pénélope Desroys Du Roure, Valérie Laurent-Matha, Hanane Mansouri, Marta Jarlier, Pierre Martineau, et al.

Anti-cathepsin D immunotherapy triggers both innate and adaptive anti-tumour immunity in breast cancer

Running Title: Antibody-based immunomodulatory therapy of breast cancer

Timothée David[1], Aude Mallavialle[1], Julien Faget[1], Lindsay B Alcaraz[1], Marion Lapierre[1], Pénélope Desroys du Roure[1], Valérie Laurent-Matha[1], Hanane Mansouri[1,2], Marta Jarlier[3], Pierre Martineau[1], Pascal Roger[1,4], Séverine Guiu[1,5], Thierry Chardès[1,6*], Emmanuelle Liaudet-Coopman[1*#]

[1]IRCM, INSERM U1194, Univ Montpellier, ICM, Montpellier, France.

[2]RHEM, IRCM, Montpellier, France.

[3]Biometry Department, ICM, Montpellier, France.

[4]Department of Pathology, CHU Nîmes, Nîmes, France.

[5]Department of Medical Oncology, ICM, Montpellier, France.

[6]CNRS, Centre national de la recherche Scientifique, Paris, F-75016, France

*These authors contributed equally to this work.

 # Corresponding author: E Liaudet-Coopman

IRCM - Inserm U1194

208, rue des Apothicaires

F-34298 Montpellier Cedex 5, France

E-mail: emmanuelle.liaudet-coopman@inserm.fr

ACKNOWLEDGMENTS

This work was supported by a public grant overseen by the French National Research Agency (ANR) as part of the "Investissements d'Avenir" program (reference: LabEx MabImprove ANR-10-LABX-53-01), University of Montpellier, Inserm Transfert, Région Occitanie, 'Ligue Nationale contre le Cancer', the associations 'Ligue Régionale du Gard', 'Ligue Régionale de l'Herault', and 'Ligue Régionale de la Charente Maritime. We thank Isabelle Teulon, Adeline Torro, Lucie Rubio, Salima Atis and Alexandre Pichard (Animal Facility, IRCM, Montpellier, France) for in vivo studies. We thank Cecile Dejou (MRI, Montpellier, France) for flow cytometry support. We acknowledge the "Réseau d'Histologie Expérimentale de Montpellier" - RHEM facility supported by SIRIC Montpellier Cancer Grant INCa_Inserm_DGOS_12553, the European regional development foundation and the Occitanie region (FEDER-FSE 2014-2020 Languedoc Roussillon), REACT-EU (Recovery Assistance for Cohesion and the Territories of Europe), IBiSA and Ligue contre le cancer for processing/analyzing our animal tissues with expertise. We thank Julie Constanzo (IRCM, Montpellier France) for her help with TUBO cell line. We thank Hervé Watier (University of Tours, France), Pierre Martineau (IRCM, Montpellier, France), Mireia Pelegrin (IRMB, Montpellier, France), Gilles Thibault (GICC, Tours, France), Jean-Marie Piot (University of La Rochelle, La Rochelle, France) for helpful discussions and support.

Disclosure of Potential Conflicts of Interest: No potential conflicts of interest were disclosed by all authors

Abstract

Background and purpose: Triple-negative breast cancer (TNBC) has poorer outcomes than other breast cancer (BC) subtypes, including $HER2^+$ BC. Cathepsin D (CathD) is a poor prognosis marker overproduced by BC cells and hypersecreted in the tumour microenvironment with tumour-promoting activity. Here, we characterized the immunomodulatory activity of the anti-CathD antibody F1 and of its improved Fab-aglycosylated version (F1M1) in immunocompetent mouse models of TNBC (C57BL/6 mice harbouring E0771 cell grafts) and HER2-amplified BC (BALB/c mice harbouring TUBO cell grafts).

Experimental approach: CathD expression was evaluated by western blotting and immunofluorescence, and antibody binding to CathD by ELISA. The antibody anti-tumour efficacy was investigated in mouse models. Immune cell recruitment and activation were assessed by immunohistochemistry, immunophenotyping, and RT-qPCR.

Key results: Both F1 and F1M1 antibodies remodelled the tumour immune landscape. Both antibodies promoted the innate antitumour immunity by preventing the recruitment of immunosuppressive M2-polarized tumour-associated macrophages (TAMs) and by activating natural killer cells in the tumour microenvironment of both models. This translated into a reduction of T-cell exhaustion markers in the tumour microenvironment that could be locally supported by enhanced activation of anti-tumour antigen-presenting cell (M1-polarized TAMs and cDC1 cells) functions. Both antibodies inhibited tumour growth in the highly-immunogenic E0771 model, but only marginally in the immune-excluded TUBO model, indicating that anti-CathD immunotherapy is more relevant for BC with a high immune cell infiltrate, as often observed in TNBC.

Conclusion and implication: Anti-CathD antibody-based therapy triggers the anti-tumour innate and adaptive immunity in preclinical models of BC, and is a promising immunotherapy for immunogenic TNBC.

Keywords: breast cancer, antibody-based therapy, immunomodulation, protease, tumour microenvironment, anti-tumour immunity, TNBC

Key messages

What is already known:

- Triple-negative breast cancer has poorer outcomes compared with other breast cancer subtypes
- The protease cathepsin D is a target for antibody-based therapy in triple-negative breast cancer

What this study adds:

- Anti-Cathepsin D antibodies activate the innate and adaptive anti-tumour immunity in immunocompetent mouse models of breast cancer

Clinical significance:

- Anti-Cathepsin D antibodies represent a promising immunotherapy for patients with immunogenic triple-negative breast cancer

1 INTRODUCTION

Triple-negative breast cancers (TNBC; 15% of all breast cancers, BC) are defined by the lack of oestrogen receptor, progesterone receptor and HER2 expression/amplification (Bianchini, De Angelis, Licata & Gianni, 2022). The prognosis of patients with TNBC is poor, mainly due to the disease heterogeneity and lack of targeted therapies. Immunotherapies are an interesting strategy for TNBC, which is classified as an immunogenic BC subtype due to its high tumour mutational burden and presence of immune cell infiltrates (Barroso-Sousa et al., 2020; Wojtukiewicz, Pogorzelska & Polityńska, 2022). The median tumour mutational burden, which is the main source of neoantigens to induce anti-tumour immunity, is higher in TNBC than in other BC subtypes, including the HER2-amplified BC subtype (Barroso-Sousa et al., 2020). In metastatic TNBC, immune checkpoint inhibitors (ICI) (anti-PD-1 and anti-PD-L1 antibodies) and chemotherapy have improved survival in patients with PD-L1-expressing tumours (Cortes et al., 2022; Emens et al., 2021). ICI are also a relevant option for patients with HER2-positive BC in metastatic, neoadjuvant and adjuvant settings (Kyriazoglou et al., 2022). However, more investigations are needed to understand how to increase ICI efficacy in BC and to better characterize the immune landscape in responders (Majidpoor & Mortezaee, 2021; Uchimiak, Badowska-Kozakiewicz, Sobiborowicz-Sadowska & Deptala, 2022). Antibody-based therapies that modulate the recruitment, activation and immunosuppression of immune cells in the tumour microenvironment could also represent an interesting option (Bianchini, De Angelis, Licata & Gianni, 2022; Wojtukiewicz, Pogorzelska & Polityńska, 2022).

The aspartic protease cathepsin D (CathD), a poor prognostic marker in BC (Kang et al., 2020) and TNBC (Huang, Liu, Chen, Liu & Shao, 2013; Mansouri et al., 2020), is overproduced by BC cells and hypersecreted in the tumour microenvironment (Vignon, Capony, Chambon, Freiss, Garcia & Rochefort, 1986). CathD exhibits tumour-promoting activity in BC (Fusek & Vetvicka, 1994; Glondu, Liaudet-Coopman, Derocq, Platet, Rochefort & Garcia, 2002; Hu, Roth, Brooks, Luty & Karpatkin, 2008; Ketterer et al., 2020; Zhang, Zhang & Song, 2018). In BC, extracellular CathD displays pro-tumour activities through proteolysis at acidic pH and also non-proteolytic mechanisms (Benes, Vetvicka &

Fusek, 2008; Khalkhali-Ellis & Hendrix, 2014; Masson et al., 2010). Secreted CathD can modify the local extracellular matrix by cleaving chemokines (Hasan et al., 2006; Wolf, Clark-Lewis, Buri, Langen, Lis & Mazzucchelli, 2003), growth factors, collagens, fibronectin, proteoglycans, the matricellular protein SPARC (Alcaraz et al., 2021), protease inhibitors (*e.g.,* cystatin C (Laurent-Matha et al., 2012), PAI 1 (Maynadier, Farnoud, Lamy, Laurent-Matha, Garcia & Rochefort, 2013)), or by activating the cathepsin B and L precursors (Benes, Vetvicka & Fusek, 2008). It can also promote BC cell proliferation *via* its pro-peptide (Vetvicka, Vetvickova, Hilgert, Voburka & Fusek, 1997). It can trigger breast fibroblast outgrowth upon binding to the LRP1 receptor (Beaujouin et al., 2010; Derocq et al., 2012), and induces endothelial cell proliferation and migration *via* the ERK and AKT signalling pathways (Pranjol, Gutowski, Hannemann & Whatmore, 2017). Therefore, CathD massively secreted in BC could represent a novel molecular target. However, when CathD regulation is affected, it can contribute to many disorders. Indeed, CathD deficiency or downregulation in humans is associated with neuronal ceroid lipofuscinosis, indicating its non-redundant essential role in protein catabolism and cellular homeostasis maintenance (Ketscher, Ketterer, Dollwet-Mack, Reif & Reinheckel, 2016; Mijanovic et al., 2021; Siintola et al., 2006). Hence, the concomitant inhibition of intracellular and extracellular CathD with cell-permeable chemical drugs could be toxic (Mijanovic et al., 2021). Antibodies targeting only extracellular Cath-D in BC could bypass this toxicity. It was recently reported that CathD is a potent target for antibody-based therapy in TNBC (Ashraf et al., 2019). Due to its immunomodulatory activity, the anti-CathD antibody F1 could represent a promising option for patients with chemotherapy- and/or ICI-resistant TNBC (Ashraf et al., 2019). However, the overall impact of anti-CathD antibody-based therapy on immune cell recruitment and activation in fully immunocompetent mouse models remained unknown. Here, to decipher the potential therapeutic benefit of protease-specific antibodies in pre-clinical settings, we compared for the first time the antitumour efficacy and immunomodulatory activity of anti-CathD antibodies in two fully immunocompetent mouse models of highly immune infiltrated TNBC and immune-excluded HER2-amplified BC.

2 METHODS

2.1 Materials

The anti-mouse CathD antibody against the 52-, 48-, 34-kDa forms was from Bio-Techne (#AF1029, R&D Systems - Minneapolis, MN). The HRP-conjugated anti-mouse F(ab)2 (#115-036-072) was from Jackson ImmunoResearch (West Grove, PA). The HRP substrate reagent was from Bio-Techne (R&D Systems, #DY999). The anti-HSC70 antibody (#sc-7293) was from Santa Cruz BioTechnology (Dallas, TX). The fluorescent-conjugated anti-mouse (#922-32210) and anti-goat (#926-68071) antibodies were from LI-COR Biosciences (Lincoln, NE). Injectable D-luciferin (#122799-5) was from Perkin Elmer (Waltham, MA). The mouse IgG2a isotype control antibody (C1.18.4, #BE0085) was from BioXCell (Lebanon, NH). Collagenase IV (#C5138) and DNase I (#11284932001) were from Sigma-Aldrich (St Louis, MO). Mouse Fc Block (#130-097-575) was from Miltenyi Biotec (Bergisch Gladbach, Germany). Hoechst (#33342) was from Thermo Fisher Scientific (Waltham, MA). The AF488-conjugated anti-human IgG (#A11013) was from Life Technologies (Carlsbad, CA). The fluorescent-conjugated antibodies against CD11b (clone M1/70, #101205), CD3 (clone 17A2, #100205), PD-L1 (clone 10F.9G2, #135228), F4/80 (clone QA17A29, #157308), CD16 (clone S17014E, #158005), Ly6G (clone 1A8, #127621), NKp46 (clone 29A1.4, #1377631), CD11c (clone N418, #117330), PD-1 (clone 29F.1A12, #103044), CD206 (clone C068C2, #141721), B220/CD45R (clone RA3-632, #103241), and LAG3 (clone C9B7W, #125219) were from Biolegend (San Diego, CA). The antibody against Ly6C (clone REA796, #130-111-920) was from Miltenyi Biotec; the antibodies against CD4 (clone GK1.5, #565974), CD8 (clone 53-6.7, #748535), and CD45 (clone 30-F11, #612975) were from BD Biosciences (Franklin Lakes, NJ). Viakrome IR 808 (#C36628) was from Beckman Coulter (Brea, CA). Mouse F1M1 IgG2a, mouse F1 IgG2a, and human F1M1 IgG1 were constructed from the scFv (F1, F1M1) sequences by gene synthesis, expressed in the Chinese hamster ovary cell line, and purified on protein-A HiTrap columns (GE Healthcare) by Evitria AG (Schlieren, Switzerland).

2.2 Tumour cell lines

The E0771Luc cell line, transformed to constitutively express luciferase as reporter, was kindly provided by Dr. C-L. Tomasetto (IGBMC, Strasbourg, France). Lentiviral particles were obtained by co-transfection of the pLENTI PGK Blast vector with three packaging plasmids (pLP1, pLP2, and pLP/VSVG) (Invitrogen, Carlsbad, CA) in the 293T cell line. Then, E0771Luc cells were incubated with viral particles, supplemented with 10 µg/ml polybrene and 20 mM HEPES. Luciferase expression was assessed in blasticidin (5 µg/ml)-resistant cells by bioluminescence. E0771Luc cells (E0771 cells hereafter) were cultured in RPMI1640 with 10% foetal calf serum (FCS) (Eurobio Scientific – Les Ulis, France) and 10 mM HEPES, pH=7.5 (Gibco). The E0771 cell line is derived from spontaneous tumours in C57BL/6 mice and is most often presented as a TNBC model (Johnstone et al., 2015; Liu et al., 2016; Perez-Lanzon et al., 2023), although it is sometimes considered a C57BL/6-derived luminal B mammary cancer cell line (Le Naour et al., 2020). The 4T1 cell line, kindly provided by A. Pèlegrin (IRCM, Montpellier, France), was cultured in DMEM/GlutaMAX, 10% FCS (Eurobio Scientific). The TUBO cell line, kindly provided by F. Cavallo (DBMSS, Torino, Italy), was cultured in DMEM/GlutaMAX, 20% FCS (Eurobio Scientific). The TUBO line is a cloned cell line derived from transgenic BALB/c mice that express the rat HER2/neu oncogene (Rovero et al., 2000). All cell lines were mycoplasma-free, determined using the MycoAlert™ detection kit (Lonza, Switzerland). To produce 48h-supernatant containing secreted CathD, cells were grown to 60% confluence, and left in medium with FCS for 48h. Conditioned medium was centrifuged at 800 x g for 5min.

2.3 Sandwich ELISA

First, 96-well plates were coated with an anti-CathD antibody (#AF1029, Bio-Techne) in PBS (100 ng/well) at 4°C overnight. After blocking non-specific sites with PBS/0.1% Tween 20/1% BSA, CathD-containing supernatants from E0771 or TUBO cells were added at 37°C for 2h. After washes in PBS/0.1% Tween 20, two-fold serial dilutions of F1 or F1M1 (initial concentration: 4224 nM) in PBS were added at 37°C for 2h, followed by washes in PBS/0.1% Tween 20, and incubation with a HRP-

conjugated anti-mouse F(ab)2 (1/2000) at 37°C for 2h. Plates were rinsed four times in PBS/0.1% Tween 20, and 50 µl/well of TetraMethylBenzidine substrate (#34028, ThermoFisher) was added at room temperature in the dark for 10-30min. The reaction was stopped with 50 µl/well of 2N H_2SO_4 and optical density was read at 450 nm. GraphPad Prism 8 (GraphPad Software, RRID:SCR_002798), was used to calculate the EC50 of the antibodies. Five independent assays with three replicates were performed for cancer cell lines.

2.4 Western blotting

Cell lysates were harvested in lysis buffer (50 mM HEPES pH 7.5, 150 mM NaCl, 10% glycerol, 1% Triton X-100; 1.5 mM $MgCl_2$, 1 mM EGTA) supplemented with cOMPLETE™ protease inhibitor cocktail (#4693116001, Roche, Switzerland) at 4°C for 10min. Protein concentration was determined with the DC protein assay (Bio-Rad). Then, protein samples (20 µg of cell lysates, 40 µL of cell supernatants, 5 µg of tumour lysates) were separated on 13.5% SDS-PAGE and transferred to PVDF membranes (#IPFL85R, Merck Millipore, Burlington, MA) by liquid-phase transfer at 4°C for 90min. After transfer, membranes were blocked with 100 mM Tris buffer, pH 7.4, 150 mM NaCl, 0.1% Tween 20 (TBS-T) and 3% BSA at room temperature for 1h, followed by incubation with anti-HSC70 or anti-CathD antibodies at 4°C overnight. After TBS-T washes, membranes were incubated with secondary fluorescent-conjugated anti-mouse or anti-goat antibodies in TBS-T/3% BSA at room temperature for 1h, followed by image acquisition with a LI-COR Odyssey imager, according to the manufacturer's instructions.

2.5 Animals

All animal care, ethical principles and experimental procedures were performed in compliance with the French regulations and ethical guidelines for experimental animal studies in an accredited establishment (Agreement No. #31135-2021042212479661). Animal studies are reported in compliance with the ARRIVE guidelines (Percie du Sert et al., 2020), and with the recommendations made by the British Journal of Pharmacology (Lilley et al., 2020). Female C57BL/6N and BALB/c (6-

weeks old) were purchased from Charles River (Wilmington, MA). Mice used in the experiments were 8-weeks old (20g). Mice (5 mice per cage) were kept in individually ventilated cages (transparent and with top filter-isolator) with standard bedding at a constant temperature of 23 °C and 40-60% humidity with 12h light/darkness cycle in a specific pathogen-free conditions with food and water at will. All the animal studies were designed to generate groups of equal size using randomisation and blinded analysis. The different group sizes are due to the purpose of unexpected individual losses during the process.

2.6 Orthotopic and subcutaneous tumour growth

E0771 cells (2.5×10^5 in PBS) were injected in the mammary fat pad between the fourth and fifth mammary glands of 8-week-old female C57BL/6N mice (Charles River, Wilmington, MA). After 2 days, tumour-bearing mice with similar E0771 cell bioluminescence were randomized in three treatment groups: isotype control C1.18.4 (15 mg/kg), F1 (15 mg/kg), or F1M1 (15 mg/kg) (all by intraperitoneal injection three times per week until day 33). For bioluminescence harmonization, at day 2 post-graft, 200 µL luciferin (10mg/mL) was injected in anaesthetized grafted C57BL/6N mice followed by imaging using an IVIS Lumina II camera (Caliper LifeSciences, Waltham, MA). Bioluminescence was quantified with the Living Image® v4.5.2.18424 software.

TUBO cells ($3.0\text{x}10^5$ in PBS) were injected subcutaneously in the right flank of 8 week-old female BALB/cN mice (Charles River). At day 2 post-graft, tumour-bearing mice were treated with isotype control C1.18.4 (15 mg/kg), F1 (15 mg/kg) or F1M1 (15 mg/kg) by intraperitoneal injection 3 times per week until day 21. Tumours were measured using a calliper and volume was calculated with the formula V = (tumour length × tumour width^2)/2. Mice were sacrificed (CO_2, 5 min), and tumours, draining lymph nodes (dLNs), and peripheral blood lymphocytes (PBLs) were collected for immunophenotyping. Tumour samples were frozen in liquid nitrogen for RNA extraction.

2.7 Quantitative RT-PCR

Total RNA was extracted using the Quick-RNA Mini Prep kit (#R1054, Zymo Research – Irvine, CA), according to the manufacturer's instructions. Reverse transcription of total RNA was performed at 37°C using the Transcriptase Inverse SuperScript III (Invitrogen) and random hexanucleotide primers (Promega). Real-time quantitative PCR analyses were performed on a Light Cycler 480 ONEGreen FAST pPCR Premix (#OZYA008-200XL, Ozyme – Saint-Cyr-l'Ecole, France) and a LightCycler 480 apparatus (Roche Diagnostics – Basel, Switzerland). The PCR product integrity was checked by melting curve analysis. Expression data were normalized to the amplification data for the reference gene *RPS9*. Primers (Euromedex – Souffelweyersheim, France) and their sequences are in Table S1. The experiments were performed in triplicate with more than 5 animal per cohort.

2.8 Isolation of tumour-infiltrating cells and immunophenotyping by 17-color flow cytometry

Tumours were enzymatically and mechanically digested in gentleMACS™ C-Tubes (#130-093-237, Miltenyi Biotec) that contained a mixture of collagenase IV (1 mg/ml) and DNase I (200 U/ml) in RPMI using a gentleMACS™ Octo Dissociator (Miltenyi Biotec) at 37°C (two incubations of 19.5 min and 5.5 min). After digestion, tumour suspensions were passed through a 70 µm nylon cell strainer (#22-363-548, Fisher Scientific, Waltham, MA), centrifuged and resuspended in FACS buffer (PBS pH 7.2, 0.5% FBS, and 0.02% sodium azide). dLNs were mechanically dissociated in PBS, and re-suspended in FACS buffer. Then, red blood cells were removed by adding 10 volumes of ammonium-chloride-potassium lysing buffer, and PBLs were recovered by centrifugation, washed with PBS and resuspended in FACS buffer. Cells were blocked with FACS buffer containing 1% (v/v) of mouse Fc Block, and stained with fluorescent-conjugated antibodies, followed by washes in FACS buffer, and fixation with 1% paraformaldehyde in PBS. Samples were analysed by flow cytometry using a Beckman and Coulter CytoFLEX LX 17-color flow cytometer. Immune cell populations from tumours were analysed using the following 17-color flow cytometry panel: Viakrome IR 808, and antibodies against CD45, CD11b, F4/80, CD206, CD3, CD4, CD8, Ly6G, Ly6C, NKp46, CD11c, B220, CD86, CD16, PD1, and PDL1. Living immune cells were defined as Viakrome IR 808^- and $CD45^+$. TAMs were defined as $CD45^+$ $CD11b^+$ $F4/80^+$; the

M1-TAM subset as F4/80^{+} CD206^{-} CD11c^{+}; the M2-TAM subset as F4/80^{+} CD206^{+}. Conventional DCs (cDCs) were defined as CD45^{+} CD3^{-} Ly6G^{-} B220^{+} CD11c$^{+/hi}$; the cDC2 subset as CD11c$^{+/hi}$ CD8^{-} CD11b^{+}; the cDC1 subset as CD11c$^{+/hi}$ CD8^{+} CD11b^{-}. B cells were defined as CD45^{+} F4/80^{-} CD3^{-} Ly6G^{-} Ly6C^{-} CD11c^{-} B220^{+}. NK cells were defined as CD45^{+} F4/80^{-} CD3^{-} Ly6C^{-} Ly6G^{-} CD11b$^{lo/+}$ NKp46^{+}. T cells were defined as CD45^{+} F4/80^{-} CD3^{+}; CD8^{+} T cells as CD3^{+} CD8^{+}; and CD4^{+} T cells as CD3^{+} CD4^{+}. Functional markers (CD86, CD16, PDL1, PD1) were studied in the relevant immune cell subpopulations. Immune cells from PBLs and dLNs were analysed using the following 17-color flow cytometry panel: Viakrome IR 808, and antibodies against CD45, CD3, CD4, CD8, CD11b, Ly6G, Ly6C, NKp46, CD11c, B220, CD16, PDL1, and LAG3. In PBLs, living immune cells were defined as Viakrome IR 808^{-} and CD45^{+}. T cells were defined as CD45^{+} CD3^{+}; CD8^{+} T cells as CD3^{+} CD8^{+}; and CD4^{+} T cells as CD3^{+} CD4^{+}. NK cells were defined as CD45^{+} CD3^{-} CD11b$^{+/lo}$ NKp46^{+}. Functional markers (CD16, LAG3, PDL1) were studied in the relevant immune cell subpopulations. Events were analysed with FlowJo 10.8.1.

2.9 Fluorescence microscopy

Paraffin-embedded E0771 and TUBO cell graft tissue sections were deparaffined, rehydrated, rinsed and saturated in PBS with 5% FCS at 4°C overnight. Sections were incubated with 25 µg/mL F1M1 (human IgG1 format), followed by incubation with AF488-conjugated anti-human IgG (#A11013). Nuclei were stained with 0.5 µg/mL Hoechst 33342. Images were acquired with a x63 Plan-Apochromat objective and a Zeiss Axio Imager light microscope for each tumour tissue from 5 mice for E0771 and for TUBO tumours.

2.10 Immunohistochemistry

E0771 and TUBO tumour grafts were collected and fixed in 10% neutral buffered formalin for 24h, dehydrated, and embedded in paraffin. For immunostaining, xenograft sections (3-µm thick) were deparaffinized, rehydrated and subjected to heat induced antigen retrieval with CC1 buffer (Ventana, cat# 950-124) for CD3 detection and with pH6 buffer (Agilent, EnVision FLEX Target Retrieval Solution

Low, #K800521-2) for CD45 and F4/80 detections. IHC was performed on a VENTANA Discovery Ultra automated staining instrument (Ventana Medical Systems), using VENTANA reagents, according to the manufacturer's instructions. After neutralization of endogenous peroxidase activity, sections were incubated with anti-CD45 (Bioscience, #14-0451-82, clone 30-F11), anti-CD3e (Roche, #790-4341, clone EGV6) or F4/80 (Invitrogen, #MF48000, clone BM8) antibodies for 60min. Signal enhancement was performed using the OmniMap anti-rabbit HRP Kit (Roche, #5269679001) for CD3e, and rabbit anti-rat IgG (H+L) as the secondary antibody (Thermo Scientific, #31219) and the OmniMap anti-rabbit HRP Kit for CD45 and F4/80 staining. Slides were incubated with DAB (Roche, #05266645001) then counterstained with haematoxylin II (Roche, #790-2208) for 8 min, followed by Bluing reagent (Roche, #760-2037) for 4 min. Slides were then dehydrated in a Leica autostainer and coverslipped with Pertex mounting medium with CM6 coverslipper (Microm). Slides were digitalized with a Hamamatsu NanoZoomer 2.0-HT scanner by MRI platform and images were visualized with the NDP.view 1.2.47 software. For each tumour tissue, histological sections were evaluated for 5 mice per group for each antibody.

2.11 Statistical analyses

The data and statistical analysis comply with the recommendations of the *British Journal of Pharmacology* on experimental design and analysis in pharmacology (Curtis et al., 2018). Additional data from two different models were provided to validate the results. In our in vivo analysis, the size of independent groups was superior to 5 (exact numbers are provided in the figure legends).

Results are expressed as mean ± SEM. A linear mixed regression model was used to determine the relationship between tumour growth and number of days post-graft. The variables included in the fixed part of the model were: number of days post-graft and treatment groups. Their interaction was also evaluated. Random intercepts and random slopes were included to take into account the time effect. The model coefficients were estimated by maximum likelihood. The statistical analyses for linear mixed regression model for tumour growth were done with STATA 13.0. The Mann-Whitney *t*

test was used for pairwise comparisons. Statistical analysis were performed using GraphPad Prism 8 (GraphPad Software, RRID:SCR_002798). All outliers were included in data analysis. *P* <0.05 values were considered indicative of statistical significance. All studies followed the editorial on experimental design and analysis in pharmacology (Curtis et al., 2018) and followed the BJP checklist for Design and Analysis.

2.12 Nomenclature of targets and ligands

Key protein targets and ligands in this article are hyperlinked to corresponding entries in the IUPHAR/BPS Guide to PHARMACOLOGY http://www.guidetopharmacology.org, and are permanently archived in the Concise Guide to PHARMACOLOGY 2021/22(Alexander et al., 2021).

3 RESULTS

3.1 CathD expression and secretion in preclinical mouse BC models

Analysis of CathD expression and secretion showed expression mainly of the 48-kDa intermediate chain and to a lesser extent of the mature 34-kDa heavy chain in E0771 and 4T1 cells (TNBC), and in HER2-amplified TUBO (BC) cells (Lysates; Figure 1A; Figure S1). We observed the 52-kDa CathD precursor in the supernatant (SN) of E0771 and TUBO cells (Figure 1A), but not of 4T1 cells (Figure S1). CathD was also expressed in E0771 and TUBO cell grafts (Figure 1B) where it showed intense and punctuate staining (Figure 1C) that mirrored the expression pattern in BC biopsy samples (Ashraf et al., 2019). Therefore, EO771 and TUBO cells are suitable models to study the antitumour and immunomodulatory activity of anti-CathD antibodies in syngeneic mouse models of basal-like TNBC and HER2-amplified BC, respectively.

3.2 The mouse IgG2a-formatted F1 and Fab-aglycosylated F1M1 antibodies bind to secreted mouse CathD

We formatted the anti-CathD IgG1 human antibody F1 (Ashraf et al., 2019) in the murine IgG2a format to investigate its anti-tumour effect and immunomodulatory activity in fully immunocompetent mouse models of BC. We also generated the new murine IgG2a anti-CathD antibody F1M1 with point mutations (one in VL CDR3 and one in VH FR3) to abrogate Fab N-glycosylation that may lead to the production of glycoforms associated with the risk of immunogenic responses in patients, as described for cetuximab (van de Bovenkamp, Hafkenscheid, Rispens & Rombouts, 2016). The migration profiles of F1 and F1M1 showed that the molecular weight of the light and heavy chains was lower in F1M1 than F1, as expected due to reduced glycosylation (Figure S2). Sandwich ELISA using CathD secreted from E0771 and TUBO cells showed that F1 and F1M1 had good binding capacities (EC_{50}=43.5 nM and 33.8 nM for F1 and EC_{50}=0.9 nM and 0.2 nM for F1M1, respectively) (Figure 1D). The lower EC_{50} of F1M1 indicated that the two-point mutations leading to Fab aglycosylation enhanced F1M1 capacity to recognize mouse CathD, possibly because VL-CDR3 glycosylation decreased F1 affinity due to steric hindrance. Therefore, both F1 and F1M1 were investigated *in vivo*.

3.3 Immunological profile of the TNBC and HER2-amplified BC preclinical models

To investigate the anti-tumour and immunomodulatory effects of our anti-CathD antibodies in pre-clinical settings, we established an orthotopic TNBC model by grafting basal-like p53-mutated E0771 cells in C57BL/6 mice (Johnstone et al., 2015), and a HER2-amplified BC model by grafting TUBO cells in BALB/c mice (Rovero et al., 2000). These two CathD-secreting cell lines readily formed tumours upon grafting (Figure S3A-B). We then analysed tumour-infiltrating immune cells in untreated E0771 and TUBO cell grafts by immunohistochemistry. We observed many tumour-infiltrating CD45$^+$ immune cells, F4/80$^+$ macrophages, and CD3$^+$ T cells in E0771 cell-derived tumours (Figure 1E). In TUBO-derived tumours, CD45$^+$ immune cells were less frequent and F4/80$^+$ macrophages were present only at the tumour-stroma interface with very few CD3$^+$ T cells, suggesting immune cell exclusion (Figure 1F). We further analysed the tumour immune infiltrate in untreated E0771 and TUBO cell grafts by 17-color flow cytometry analysis (Figure S4 and Figure S5). The number of CD45$^+$ immune cells was higher in

E0771 than TUBO cell grafts (20% and 7.2% of $CD45^+$ cells relative to all living cells in the grafts, respectively) (Figure 1G-H, left panels). E0771 cell grafts were infiltrated mainly by TAMs (55.3% of all $CD45^+$ cells), particularly M2-polarized cells (40.7% of all $CD45^+$ cells), followed by NK cells (7.4% of all $CD45^+$ cells), and $CD4^+$ and $CD8^+$ T cells (2.8% and 2.8% of all $CD45^+$ cells, respectively) (Figure 1G, middle and right panels), as observed in human TNBC (Fan & He, 2022). In TUBO cell grafts, the percentages of TAMs (28.2% of all $CD45^+$ cells), of NK cells (3.2% of all $CD45^+$ cells), and of $CD4^+$ and $CD8^+$ T cells (1% and 0.03% of all $CD45^+$ cells, respectively), were lower (Figure 1H, middle and right panels). In these tumours, neutrophils were the main immune cells (55.3% of all $CD45^+$ cells vs 13% in E0771 cell grafts) (Figure 1H, middle panel, and Figure 1G, left panel). Direct comparison of the percentage of immune cell subpopulations among all living cells in the E0771 and TUBO cell grafts reinforced the findings that the E0771 cell-based model displayed strong immune cell infiltration, mainly by the myeloid and lymphoid compartments, compared with the TUBO cell-based model that showed lower tumour immune infiltration, mainly by neutrophils (Figure S3C).These results suggested that the E0771 cell-based TNBC model could be defined as highly immunogenic with a potential anti-tumour effector response, whereas the TUBO cell-based BC model displayed hallmarks of immunosuppression with immune exclusion.

3.4 Anti-Cath-D antibody-based therapy is more effective in the immune-prone TNBC model than in the immune-excluded HER2-amplified BC model

First, we studied the antitumour effects of F1 and F1M1 in the immune-prone TNBC model (E0771 cells). We treated tumour-bearing mice with similar luciferase bioluminescence levels (Figure S6), with F1, F1M1, or C1.18.4 isotype control (CTRL) (15 mg/kg, 3 times per week for 31 days; n=9 mice/group). F1 and F1M1 significantly delayed tumour growth compared with control (Figure 2A). Only 1/9 mice in the F1 group and 2/9 mice in the F1M1 group did not respond to treatment (Figure 2B). At day 33 (sacrifice day), tumour volume was significantly reduced by 51.9% in the F1 group and by 61.9% in the F1M1 group compared with control (Figure 2C). Moreover, mice treated with F1 and F1M1 gained

weight like the isotype control (Figure 2D), and displayed normal activities without prostration, suggesting no apparent toxicity. Drug-induced neutropenia is a potentially serious and life-threatening adverse event that may occur after therapy with various agents, including antibodies. Analysis by 17-color flow cytometry of blood from mice grafted with E0771 cells (Figure S7A) showed that neutrophil count at day 33 was not affected, indicating the absence of neutropenia (Figure S8).

Then, we evaluated F1 and F1M1 in the HER2-amplified BC model representative of immunosuppression and immune exclusion. At day 2 post-graft, we randomly divided mice in three groups: F1, F1M1, and C1.18.4 isotype control (CTRL) (15 mg/kg) (intraperitoneal injection 3 times per week for 17 days) (n=12 mice/group). Tumour growth was not significantly reduced in the F1 and F1M1 groups compared with the control group (Figure 2E). Moreover, 3/12 mice in the F1 group and 1/12 mice in the F1M1 group did not respond to treatment (Figure 2F). At day 19 (sacrifice day), tumour volume was reduced by 26.4% in the F1 group and by 15.6% in the F1M1 group compared with the control group (Figure 2G). Mice in all groups gained weight (Figure 2H) and displayed normal activities without prostration. Analysis by 17-color flow cytometry analysis of blood from mice grafted with TUBO cells at day 19 (Figure S9A) showed no neutropenia in all groups (Figure S10). Altogether, these findings indicated that anti-Cath-D antibody-based therapy is effective in the highly-immunogenic TNBC model, but only marginally effective in the immune-excluded HER2-amplified BC model.

3.5 Anti-CathD antibody-based therapy rebalances TAM recruitment and activation in tumours

To study F1 and F1M1 immunomodulatory properties, we first analysed by 17-color flow cytometry the immune infiltrates of E0771 cell grafts at treatment end, using the gating procedure described in ~~Figure~~ S4. We focused on TAMs because they have been associated with TNBC progression and relapse (Chang, Lam, Hsu & Jiang, 2021). TAM ($F4/80^+$ $CD11b^+$ cells) percentage within the immune $CD45^+$ cell population significantly decreased by 26.9% and 28.3% in F1- and in F1M1-treated animals compared with the C1.18.1 control (Figure 3A). Moreover, the proportion of $F4/80^+$ $CD206^+$ M2-polarized TAMs (with pro-tumorigenic functions) (Tariq, Zhang, Liang, Ding, He & Yang, 2017) within the immune

F4/80^{+} CD11b^{+} TAM population significantly decreased by 33.4% and 43.5% in F1- and F1M1-treated animals compared with control (Figure 3B). Conversely, the proportion of F4/80^{+} CD206^{-} CD11c^{+} M1-polarized TAM was comparable in all groups (Figure 3C, left panel). However, the proportion of activated (CD86^{+}) M1-polarized TAMs (capable of antigen presentation) increased by 163.3% and 153.9% in F1- and F1M1-treated animals compared with control (Figure 3C, right panel). RT-qPCR analysis of tumour samples showed that the expression of the genes encoding chemokine ligand 2 (*Ccl2*) and its C-C motif chemokine receptor type 2 (*Ccr2*), which are involved in TAM recruitment (Fang et al., 2016), was significantly downregulated by 30.1% and 74.1% in the F1 group, and by 50.2% and 71.9% in the F1M1 group compared with control (Figure 3D, upper panels). Moreover, the expression level of *Il10* (immunoregulatory cytokine that could be involved in the M2-polarized TAM immunosuppressive activity) (Chang, Lam, Hsu & Jiang, 2021)), was significantly decreased by 68.2% and by 91.5% in the F1 and F1M1 groups, respectively. Similarly, expression of *Mmp9* (matricellular protease associated with extracellular matrix remodelling and BC malignancy (Dong et al., 2019), and secreted by M2-polarized TAMs in BC (Pelekanou, Villarroel-Espindola, Schalper, Pusztai & Rimm, 2018) was significantly downregulated by 66.6% and by 93.2% in the F1 and F1M1 groups, respectively (Figure 3D, bottom panels). Therefore, anti-CathD antibody-based therapy inhibited the recruitment of pro-tumour M2-polarized TAMs and increased the pool of activated anti-tumour M1-polarized TAMs in the E0771 TNBC preclinical model. In the HER2-amplified TUBO BC model, using the gating procedure described in Figure S5, the percentages of F4/80^{+} TAMs and of CD206^{+} M2-polarized TAMs were significantly reduced by 43.5% and 55.2% in the F1 group, and by 37.9% and 53.6% in the F1M1 group, respectively, compared with control (Figure S11A). Therefore, our data strongly suggest that in preclinical immunocompetent models of BC, anti-CathD antibody therapy modifies the myeloid immune population composition in the tumour microenvironment, leading to a less immunosuppressive microenvironment and the induction of the anti-tumour response.

3.6 Anti-CathD antibody-based therapy induces NK cell activation and cytotoxic activity in tumours

NK cells are frequently involved in the efficacy of antibody-based immunotherapies by triggering antibody-dependent cell-mediated cytotoxicity upon binding of the antibody fragment crystallizable (Fc) to Fcγ receptors (FcγR) on target immune cells (Souza-Fonseca-Guimaraes, 2016). Therefore, we identified and quantified NK cells (i.e. $CD45^+$ $F4/80^-$ $CD3^-$ $Ly6C^-$ $Ly6G^-$ $CD11b^{lo/+}$ $NKp46^+$ cells) in E0771 cell grafts by 17-color flow cytometry at treatment end (day 33). The percentage of NK cells within the immune $CD45^+$ cell population was comparable in the F1, F1M1, and control groups (Figure 4A, left panel). However, the percentage of tumour $NKp46^+$ NK cells that expressed the activation marker CD16 (FcγRIII) was significantly increased by 203.2% and by 172% in F1- and F1M1-treated animals (Figure 4A, right panel). RT-qPCR analysis showed that the gene encoding interleukin-15 (*Il15)*, a cytokine associated with NK cell activation (Steel, Waldmann & Morris, 2012)**,** was upregulated up to 652% and 325% in the F1 and F1M1 groups, respectively, compared with control (Figure 4B, left panel). Similarly, *Fcgr1*, *Fcgr2b*, *Fcgr3*, *Fcgr4* and *Fcgrt* (genes encoding FcγR involved in cell-mediated immunity (Cassard, Cohen-Solal, Camilleri-Broet, Fournier, Fridman & Sautes-Fridman, 2006)) were highly upregulated by 4430%, 5430%, 2046%, 2438%, and 489.4% in the F1 group, and by 4255%, 3030%, 1580%, 2276%, and 908.6% in the F1M1 group compared with control (Figure 5). *Tnf* (encoding an antitumour cytokine) (Wang, Jaw, Stutzman, Zou & Sun, 2012) was significantly upregulated by 416% and by 1580% in the F1 and F1M1 groups, respectively (Figure 4B, right panel). Conversely, in PBLs from E0771 cell-grafted mice, the percentages of NK cells and $CD16^+$ NK cells were comparable among groups, suggesting that NK cells are specifically activated within tumours upon anti-Cath-D antibody therapy (Figure S12). The proportion of tumour-infiltrating $CD16^+$ NK cells was significantly increased by 170.2% and by 175.2% in the F1 and F1M1 groups, respectively, compared with control also in the HER2-amplified TUBO BC model (Figure S11B). Altogether, our data demonstrated that anti-CathD antibody-based therapy induced NK cell activation and cytotoxic activity in tumours in preclinical immunocompetent models of BC.

3.7 Anti-CathD antibody-based therapy triggers cDC1 cell recruitment and maturation in tumours

To assess F1 and F1M1 effect on the recruitment and maturation status of cDCs, we quantified by 17-color flow cytometry cDCs (i.e. $CD45^+$ $CD3^-$ $Ly6G^-$ $B220^+$ $CD11c^{+/hi}$ cells), cDC2 (i.e. $CD11c^{+/hi}$ $CD8^-$ $CD11b^+$ cells) and cDC1 cells (i.e. $CD11c^{+/hi}$ $CD8^+$ $CD11b^-$ cells) in E0771 cell grafts at day 33. The percentages of tumour-recruited cDCs and cDC2 cells within the immune $CD45^+$ cell population were comparable in the three groups. Conversely, the proportion of cDC1 cells was significantly increased by 244% and by 311% in the F1 and F1M1 groups, respectively, compared with control (Figure 6A). Moreover, the proportion of tumour-infiltrating cDC1 cells that expressed the maturation surface marker CD86 was significantly increased by 750% and by 500% in the F1 and F1M1 groups (Figure 6B), suggesting the setting/establishment of an adaptive antitumour response. cDC1 cells are implicated in antigen presentation to major histocompatibility (MHC) class I (MHC class I) molecules, leading to activation of cytotoxic responses by $CD8^+$ T cells, and in the anti-tumour immunity in response to immunotherapies (Bottcher & Reis e Sousa, 2018). The expression of *H2d1*, *H2k1*, and beta-2-microglobulin (*B2m)* (genes encoding proteins involved in antigen presentation *via* MHC class I molecules) was significantly upregulated by 8219%, 2015% and 4561% in the F1 group, and by 13599%, 3320% and 6693% in the F1M1 group compared with control (Figure 6C). Similarly, the expression of *IL12p40,* which encodes interleukin-12 that is secreted by mature cDC1 cells and boosts the anti-tumour activity of T cells and NK cells within the tumour (Bottcher & Reis e Sousa, 2018), was upregulated by 1358% and by 11198% in the F1 and F1M1 groups, respectively (Figure 6C). Moreover, the percentage of tumour-infiltrating $CD86^+$ B cells, but not of all B cells recruited to the tumour, was significantly increased by 223.4% and by 232.8% in the F1 and F1M1 groups, respectively (Figure S13). In the HER2-amplified TUBO BC model, the percentages of tumour-infiltrating cDC1 and cDC2 cells were significantly increased by 461.8% and 296.7% in the F1 group and by 365.7% and 354.6% in the F1M1 group compared with control (Figure S11C). The percentage of tumour $CD86^+$ cDC1 cells also was significantly increased by 128.7% and 140.2% in the F1 and F1M1 groups compared with control (Figure S11D). In conclusion, anti-CathD antibody therapy triggered cDC1 recruitment and maturation in tumours to potentially promote

antigen presentation and the antitumour T-cell co-stimulation in preclinical immunocompetent models of BC.

3.8 Anti-CathD antibody-based therapy reduces T-cell exhaustion in tumours and draining lymph nodes

To analyse the recruitment and phenotype of tumour-infiltrating T cells in E0771 cell-grafted C57BL/6 mice in response to anti-CathD antibodies, we quantified by 17-color flow cytometry $CD3^+/CD4^+$ and $CD3^+/CD8^+$ T cells within the $CD45^+$ immune cell population. The proportions of $CD8^+$ and $CD4^+$ T cells were comparable in the three groups (Figure 7A-B, left panels). Immunotherapy targeting the PD-L1/PD-1 axis checkpoint blockade to rescue T cells from exhaustion has become an essential therapeutic strategy in cancers, including TNBC (Cortes et al., 2022). Therefore, we studied PD-1 and PD-L1 expression on tumour-infiltrating $CD4^+$ and $CD8^+$ T cells. PD-L1 has recently been shown to be expressed by T cells, promoting immunosuppression in the tumour environment and is related to tumour immune tolerance and the adaptive immune response (Brochez, Meireson, Chevolet, Sundahl, Ost & Kruse, 2018; Diskin et al., 2020; Zheng et al., 2022). The percentage of tumour-infiltrating $CD8^+$ and $CD4^+$ T cells that expressed the exhaustion marker PD-1 was comparable in the three groups (Figure S14). Conversely, the percentage of PD-L1-expressing tumour-infiltrating $CD4^+$ and $CD8^+$ T cells was significantly decreased by 38.7% and 29.3% in the F1 group and by 38.5% and 35.1% in the F1M1 group, compared with control (Figure 7A-B, right panels). Similarly, in dLNs, using the gating procedure described in Figure S7B, the percentage of $CD4^+$ T cells that expressed PD-L1 and lymphocyte-activation gene 3 (LAG3, another exhaustion marker) (Du, Yi, Wang, Li, Niu & Ren, 2020) was decreased by 43.9% and 78.1% and by 29.2% and 64% in the F1 and F1M1 groups (Figure S15A). $PD\text{-}L1^+$ and $LAG3^+$ $CD8^+$ T cells also were decreased by 49% and 53.5% (F1) and by 33.3% and 47.1% (F1M1) (Figure S15B), without any change in the overall T cell population (Figure S9A-B, left panels). Conversely, in PBLs using the gating procedure described in Figure S7B, only the proportion of $LAG3^+$ $CD4^+$ T cells was decreased in the F1M1 group (Figure S15C-D). These results indicate T-cell exhaustion decreases in tumours and

dLNs in E0771 cell-grafted immunocompetent mice upon anti-CathD antibody therapy. In agreement, the tumour expression levels of *Lag3* and *Tigit* (T-cell immunoreceptor with Ig and ITIM domains), two genes involved in T-cell exhaustion (Rye et al., 2022), were reduced significantly by 67.3% and 74.5% in the F1 group, and by 89.3% and 79.5% in the F1M1 group, compared with control (Figure 7C). Moreover, forkhead box P3 (*Foxp3* encoding a Treg marker) (Watanabe, Oda, Amarante & Cesar Voltarelli, 2010) and *Il4* (supporting Treg-mediated immune suppression (Yang et al., 2017)) were significantly downregulated in tumours by 65.9% and 66.4% in the F1 group, and by 74.2% and 49.8% in the F1M1 group (Figure 7D). Due the paucity of tumour-infiltrating T cells in the TUBO cell grafts (Figure 1H), the CD4/CD8 T cell phenotype could not be studied. However, PD-L1$^+$ CD4$^+$ T and PD-L1$^+$ CD8$^+$ T cells and LAG3$^+$ CD8$^+$ T cells were decreased in dLNs after treatment with F1 and F1M1 (Figure S16A-B), using the gating procedure described in Figure S9B. Collectively, our data highlight that anti-CathD antibodies restored the anti-tumour immunity by reducing T-cell exhaustion in tumours and in dLNs in E0771 cell grafts (preclinical model of TNBC). Our results also suggest that anti-CathD antibodies could reduce the tumour Treg pool in this model.

4 Discussion

Here, we characterized the immunomodulatory activity of the F1 anti-CathD antibody isolated from a library of human scFv phages (Ashraf et al., 2019) and of its improved Fab-aglycosylated version (F1M1) in immunocompetent mouse models of TNBC (C57BL/6 mice harbouring E0771 cell grafts) (Ager et al., 2015; Johnstone et al., 2015) and HER2-amplified BC (BALB/c mice harbouring HER2-amplified TUBO cell grafts) (Park et al., 2010; Rovero et al., 2000). We found that E0771 cell-derived tumours contained large populations of myeloid and lymphoid cells with high proportions of F4/80$^+$ TAMs (predominantly M2 phenotype) and CD4$^+$ and CD8$^+$ T cells, like human TNBC (Fan & He, 2022). Conversely, TUBO cell-derived tumours contained lower level of CD45+ immune cells, mainly with a neutrophil phenotype, and few myeloid (TAM) and lymphoid cells (CD4$^+$ and CD8$^+$ T cells). Moreover, the localization of CD45$^+$ immune cells, including TAM (F4/80$^+$ cells) and T cells (CD3$^+$ cells), in TUBO

grafts was mainly restricted to the tumour periphery, suggesting that TUBO cells may be an immune cell exclusion model. Both F1 and F1M1 inhibited tumour growth effectively in the highly immunogenic E0771 model, but only marginally in the immune-excluded TUBO model. This suggests that anti-CathD immunotherapy may be more relevant for BC with high $CD45^+$ cell infiltrate. The limited response to anti-CathD antibody-based therapy in the TUBO model may reflect differences in immune cell infiltration and composition, compared with the TNBC E0771 model, and to the different mouse genetic backgrounds. C57BL/6 mice and BALB/c mice are Th1- and Th2-type strains, respectively (Watanabe, Numata, Ito, Takagi & Matsukawa, 2004), suggesting that C57BL/6 mice are a more pertinent model to study the tumour cell immune responses. Other parameters, such as HER2 expression, and downstream oncogenic signalling, could contribute to the different responses to treatment (Sow et al., 2020). Nevertheless, the F1 and F1M1 immunomodulatory activity showed many similarities in the two models, including M2-polarized TAM depletion, M1-polarized TAM and NK cell activation, and cDC1 cell recruitment and activation. Although, we could not evaluate the antibody impact on T cells in TUBO cell-derived tumours because of their paucity, T-cell exhaustion was decreased in dLNs, as observed in the E0771 model.

The anti-CathD antibodies modified the balance in favour of antitumorigenic immune activity within the tumour. This suggests that CathD in the TNBC microenvironment contributes in altering the balance of effector and regulatory immune cells and signals. In the tumour microenvironment, cancer cells exert paracrine regulatory effects through multiple chemokine/cytokine and protease interactions. CathD secreted in the extracellular medium by melanoma cells can inactivate the chemotactic effect of the chemokine CCL-20 by proteolytic cleavage, thereby abrogating the recruitment of immature CCR6-expressing DCs, and possibly preventing the establishment of an effective antitumour immune response (Hasan et al., 2006). In BC, secreted CathD can enzymatically inactivate cytokines, such as macrophage inflammatory proteins -1α and -1β, thus affecting macrophage recruitment (Wolf, Clark-Lewis, Buri, Langen, Lis & Mazzucchelli, 2003). These data suggest that inactivation of chemokines and cytokines by CathD may influence regulatory mechanisms

in the tumour extracellular microenvironment, thus affecting the antitumour immune response. *In vivo*, anti-CathD antibodies might promote the anti-tumour immunity by affecting CathD-induced degradation of various cytokines, chemokines and other immune cell-related substrates involved in immune cell recruitment and activation and in their cross-talk. To our knowledge, there are few data on CathD role in the antitumour immunity *in vivo*. Our study described for the first time the impact of CathD immunotargeting *in vivo* on the antitumour immunity in immunocompetent BC models.

TAMs are the most abundant inflammatory cells in BC, and are typically M2-polarized cells with suppressive activity (Tariq, Zhang, Liang, Ding, He & Yang, 2017) linked to the production of immunoregulatory cytokines, such as IL-10 (Chang, Lam, Hsu & Jiang, 2021). M2-polarized TAMs have low presentation capacity and suppress the antitumour immunity, while M1-polarized TAMs display anti-tumour activity (Munir et al., 2021). Here, we demonstrated that F1 and F1M1 reduced the pool of tumour-infiltrating M2-polarized TAMs, and favoured the activation of M1-polarized TAMs. This may represent the general mechanism of action of anti-protease antibodies because treatment with an anti-MMP14 antibody polarized TAMs toward the antitumour M1 phenotype in the EO771 model (Ager et al., 2015). TAM polarization is tightly regulated by different processes, including the balance between cytokines and chemokines in the tumour microenvironment. Indeed, macrophages are polarized into proinflammatory M1 cells in the presence of TNFα, and into M2 cells by interleukin-4 and interleukin-10 (Munir et al., 2021). *Tnf* upregulation, and *Il4* and *Il10* downregulation in E0771 cell-derived tumours from mice treated with anti-CathD antibodies could explain the increase of activated M1-polarized and the reduction of M2-polarized TAMs. Moreover, cytokines and chemokines are implicated in TAM recruitment (Munir et al., 2021). In the E0771 model, the expression of *Ccl2* and *Ccr2*, which are strongly associated with TAM recruitment (Fang et al., 2016), was decreased as previously shown for cathepsin K (Herroon, Rajagurubandara, Rudy, Chalasani, Hardaway & Podgorski, 2013). Overall, the reduced macrophage infiltration and decreased M2-polarized TAM population in response to anti-CathD antibody treatment are in line with the ongoing TAM-targeting therapeutic strategies (Munir et al., 2021). Importantly, tumour-educated M2-polarized TAMs secrete cytokines

(e.g. TGFβ and IL-10) that induce Treg expansion and inhibit NK cell and DC activities. Therefore, the reduction of the M2-polarized TAMs upon anti-CathD immunotherapy could stimulate the adaptive antitumour immunity.

We found that F1 and F1M1 induced activation of tumour-infiltrating NKp46^{+} NK cells, particularly in the TNBC E0771 cell-based model, suggesting that antibody-dependent cell-mediated cytotoxicity of tumour cells through F1- and F1M1-FcγR interaction (particularly CD16) could contribute to the anti-CathD immunotherapy effect. This hypothesis is also supported by the increased expression of genes encoding FcγR, which are required for the induction of FcγR-mediated cytotoxicity, observed in E0771 cell-derived tumours upon F1 and F1M1 treatment. The genes encoding IL-15 (marker of NK cell activation) (Steel, Waldmann & Morris, 2012) and the pro-inflammatory anti-tumour cytokine TNFα (Wang, Jaw, Stutzman, Zou & Sun, 2012) also were upregulated in E0771 cell-derived tumours from mice treated with anti-CathD antibodies. As NK cells control mammary tumour development in EO771 cell-grafted mice (Hoover, Gullickson & Kornbluth, 2012), NK cell activation induced by anti-CathD antibody treatment may also participate in the antitumour response.

For an effective anti-tumour immune response, NK cells and T lymphocytes must recognize and destroy cancer cells. However, innate NK cells are in a pre-activated state and adaptive T lymphocytes need to be primed by APCs (e.g. DCs). NK cells are crucial for cDC1 migration and maturation in the tumour microenvironment (Bottcher et al., 2018). Here, we found that anti-CathD antibodies activated APCs, as indicated by the increased proportion of activated M1-polarized TAMs, of cDC1 recruitment and activation, and of activated B cells. Tumour growth inhibition following F1 and F1M1 treatment was associated with activation of CD206^{-} CD11c^{+} M1-polarized TAMs and CD11c$^{+/hi}$ CD8^{+} CD11b^{-} cDC1 cells in the tumour microenvironment, suggesting an improved antigen-presenting ability to induce the adaptive immunity. In agreement, genes encoding molecules involved in antigen presentation and cell-mediated immunity within the tumour (i.e. MHC class 1 molecules, β2-microglobulin, and FcγRs) were upregulated in the F1 and F1M1 groups. This indicates that anti-CathD antibody-based therapy activates APCs required to prime anti-tumour adaptive T lymphocytes.

Anti-CathD immunotherapy also reduced $CD4^+$ and $CD8^+$ T cell exhaustion in the tumour and dLNs, as indicated by the downregulation of PD-L1, LAG3 and TIGIT (exhaustion markers). In tumours, PD-L1 expression is classically associated with other immune populations (cancer cells, TAMs, APCs, myeloid-derived suppressor cells) (Zheng et al., 2018). However, recent studies have described the immunosuppressive role of PD-$L1^+$ T cells in the tumour microenvironment (Brochez, Meireson, Chevolet, Sundahl, Ost & Kruse, 2018; Diskin et al., 2020; Zheng et al., 2022). Moreover, a significant proportion of PD-$L1^+$ T cells co-express LAG3 (Diskin et al., 2020). $CD8^+$ T cells are the main tumour cell killers in the adaptive immunity, and accumulation of tumour-infiltrating $CD8^+$ T cells is associated with favourable prognosis (Fridman, Pages, Sautes-Fridman & Galon, 2012). In the E0771 model, reducing the $CD8^+$ compartment exacerbated tumour growth (Karkeni et al., 2019), whereas $CD4^+$ population evolved from a predominant Th1 phenotype at early stages to a T regulatory (Treg) subtype associated with an immunosuppressive phenotype at more advanced stages (Huang et al., 2015). Anti-cath-D immunotherapy did not favour the recruitment of $CD8^+$ T cells, but reduced their exhaustion in the TNBC model. By downregulating *Foxp3* gene expression, F1 and F1M1 could reduce the suppressive capacity of tumour-infiltrating $CD4^+$ Treg in TNBC. Indeed, in the E0771 model, intra-tumoural $CD4^+$ T cells are mostly $FOXP3^+$ Treg cells (Crosby et al., 2018), suggesting a potential role for anti-Cath-D immunotherapy in the depletion of $CD4^+$ Treg cells that support E0771 BC progression (Clark et al., 2020). In addition, by reducing T-cell exhaustion *via* PD-L1/LAG3/TIGIT downregulation, F1 and F1M1 could strengthen the antigen-presenting function of intra-tumoural DCs, and accelerate the generation of tumour-reactive $CD8^+$ T cells, as demonstrated with TLR agonists (Salmon et al., 2016) and high-motility group nucleosome binding domain 1 (HMGN1) (Chen et al., 2021).

Comparison of the therapeutic efficacy of our anti-Cath D antibodies F1 and F1M1 in the E0771 and TUBO cell graft models suggests that their antitumour activity could be immune cell-mediated, and thus would be highly effective in combination with ICI in hot tumours. Conversely, immune-excluded tumours might require more complex management by combining other drugs. The highly immunogenic E0771 cell-based TNBC-like model represents a model of choice for testing the

combination of F1/F1M1 with anti-PD1 checkpoint inhibitors because E0771 cells express PD1 and PD-L1 (Gray et al., 2016). Moreover, anti-PD1 ICI alone leads to partial antitumour effects in the E0771 model (Kasikara et al., 2019), suggesting the interest of associating other treatments. In mice harbouring E0771 cell-derived tumours, immunotherapy combining anti-PD1 and anti-CD137 antibodies increases the number of circulating $CD8^+$ T, leading to enhanced antitumour response (Liu et al., 2016). Therefore, combining these antibodies with anti-CathD antibodies might improve the anti-tumour response in BC, as demonstrated with anti-CD137 antibodies (Liu et al., 2016) and inhibitors of the AXL family (Kasikara et al., 2019) in the E0771 model. Interestingly, pro-inflammatory cytokines, such as IL-2 or TNF-α, are frequently associated with prolonged survival of mice harbouring E0771 cell-derived tumours (Kasikara et al., 2019; Mihich & Ehrke, 2000). TNF-α expression was also increased in F1- and F1M1-treated E0771 cell-derived tumours. When associated with doxorubicin chemotherapy, TNF-α stimulates $CD8^+$ T and NK cells to induce complete tumour remission in the E0771 model (Mihich & Ehrke, 2000). This suggests that the anti-CathD antibody-chemotherapy combination could improve TNBC management. From a clinical point of view, one of the limitations of our study is that we did not compare the therapeutic effects of anti-CathD immunotherapy and of anti-PD1 therapy alone or in combination. However, as in patients with BC, particularly TNBC, PD1 inhibitors show long-term benefits (disease-free survival and overall survival) (Emens et al., 2021), we should first demonstrate the superiority of anti-CathD immunotherapy over anti-PD1 therapy alone or in combination. In summary, our study shows for the first time that anti-CathD antibody-based therapy triggers the anti-tumour innate and adaptive immunity in preclinical models of BC, and is a promising immunotherapy for patients with immunogenic TNBC.

AUTHOR CONTRIBUTIONS

TD, TC, ELC designed the experiments and prepared the manuscript. TD, AM, LBA, PDR, ML, HM, TC, ELC performed the experiments. TD, AM, LBA, VLM, MJ, PM, SG, PR, JF, TC, ELC provided material and analysed data. TD, TC, ELC analysed data and proof-read and finalized the manuscript.

DECLARATION OF TRANSPARENCY AND SCIENTIFIC RIGOUR

This declaration acknowledges that this paper adheres to the principles for transparent reporting and scientific rigour of preclinical research as stated in the *BJP* guidelines for Design & Analysis, immunoblotting and immunohistochemistry, and Animal Experimentation, and as recommended for funding agencies, publishers, and other organizations engaged with supporting research.

DATA AVAILABILITY STATEMENT

Data available on request from the authors.

List of Abbreviations

APCs: antigen-presenting cells; BC: breast cancer; CathD: cathepsin D; cDC: conventional dendritic cells; CDR3: Complementarity-determining region 3; CTRL: control; DC: dendritic cells; dLN: draining lymph nodes; FACS: Fluorescence Activated Cell Sorting**;** Fc: fragment crystallizable; FCS: foetal calf serum**;** FcγR: Fcγ receptor; FR3: framework region 3; HER2: Human Epidermal Growth Factor Receptor-2; HRP: horseradish peroxidase; IHC: immunohistochemistry; NK: natural killer cell; PBLs: peripheral blood lymphocytes; PBS: phosphate-buffered saline; RT-qPCR: quantitative reverse transcription PCR; SN: supernatant; TAM; tumour-associated macrophages; TNBC: Triple-negative breast cancer; VH: variable heavy chain; VL: variable light chain.

REFERENCES

Ager EI, Kozin SV, Kirkpatrick ND, Seano G, Kodack DP, Askoxylakis V*, et al.* (2015). Blockade of MMP14 activity in murine breast carcinomas: implications for macrophages, vessels, and radiotherapy. J Natl Cancer Inst 107.

Alcaraz LB, Mallavialle A, David T, Derocq D, Delolme F, Dieryckx C*, et al.* (2021). A 9-kDa matricellular SPARC fragment released by cathepsin D exhibits pro-tumor activity in the triple-negative breast cancer microenvironment. Theranostics 11**:** 6173-6192.

Alexander SP, Fabbro D, Kelly E, Mathie A, Peters JA, Veale EL*, et al.* (2021). THE CONCISE GUIDE TO PHARMACOLOGY 2021/22: Enzymes. Br J Pharmacol 178 Suppl 1**:** S313-S411.

Ashraf Y, Mansouri H, Laurent-Matha V, Alcaraz LB, Roger P, Guiu S*, et al.* (2019). Immunotherapy of triple-negative breast cancer with cathepsin D-targeting antibodies. J Immunother Cancer 7**:** 29.

Barroso-Sousa R, Jain E, Cohen O, Kim D, Buendia-Buendia J, Winer E*, et al.* (2020). Prevalence and mutational determinants of high tumor mutation burden in breast cancer. Ann Oncol 31**:** 387-394.

Beaujouin M, Prebois C, Derocq D, Laurent-Matha V, Masson O, Pattingre S*, et al.* (2010). Pro-cathepsin D interacts with the extracellular domain of the beta chain of LRP1 and promotes LRP1-dependent fibroblast outgrowth. J Cell Sci 123**:** 3336-3346.

Benes P, Vetvicka V, & Fusek M (2008). Cathepsin D--many functions of one aspartic protease. Crit Rev Oncol Hematol 68**:** 12-28.

Bianchini G, De Angelis C, Licata L, & Gianni L (2022). Treatment landscape of triple-negative breast cancer - expanded options, evolving needs. Nat Rev Clin Oncol 19**:** 91-113.

Bottcher JP, Bonavita E, Chakravarty P, Blees H, Cabeza-Cabrerizo M, Sammicheli S*, et al.* (2018). NK Cells Stimulate Recruitment of cDC1 into the Tumor Microenvironment Promoting Cancer Immune Control. Cell 172**:** 1022-1037 e1014.

Bottcher JP, & Reis e Sousa C (2018). The Role of Type 1 Conventional Dendritic Cells in Cancer Immunity. Trends Cancer 4**:** 784-792.

Brochez L, Meireson A, Chevolet I, Sundahl N, Ost P, & Kruse V (2018). Challenging PD-L1 expressing cytotoxic T cells as a predictor for response to immunotherapy in melanoma. Nat Commun 9**:** 2921.

Cassard L, Cohen-Solal J, Camilleri-Broet S, Fournier E, Fridman WH, & Sautes-Fridman C (2006). Fc gamma receptors and cancer. Springer Semin Immunopathol 28**:** 321-328.

Chang CM, Lam HYP, Hsu HJ, & Jiang SJ (2021). Interleukin-10: A double-edged sword in breast cancer. Tzu Chi Med J 33**:** 203-211.

Chen CY, Ueha S, Ishiwata Y, Shichino S, Yokochi S, Yang*, et al.* (2021). Combining an Alarmin HMGN1 Peptide with PD-L1 Blockade Results in Robust Antitumor Effects with a Concomitant Increase of Stem-Like/Progenitor Exhausted CD8(+) T Cells. Cancer Immunol Res 9**:** 1214-1228.

Clark NM, Martinez LM, Murdock S, deLigio JT, Olex AL, Effi C*, et al.* (2020). Regulatory T Cells Support Breast Cancer Progression by Opposing IFN-gamma-Dependent Functional Reprogramming of Myeloid Cells. Cell Rep 33**:** 108482.

Cortes J, Rugo HS, Cescon DW, Im SA, Yusof MM, Gallardo C*, et al.* (2022). Pembrolizumab plus Chemotherapy in Advanced Triple-Negative Breast Cancer. N Engl J Med 387**:** 217-226.

Crosby EJ, Wei J, Yang XY, Lei G, Wang T, Liu CX*, et al.* (2018). Complimentary mechanisms of dual checkpoint blockade expand unique T-cell repertoires and activate adaptive anti-tumor immunity in triple-negative breast tumors. Oncoimmunology 7**:** e1421891.

Curtis MJ, Alexander S, Cirino G, Docherty JR, George CH, Giembycz MA*, et al.* (2018). Experimental design and analysis and their reporting II: updated and simplified guidance for authors and peer reviewers. Br J Pharmacol 175**:** 987-993.

Derocq D, Prebois C, Beaujouin M, Laurent-Matha V, Pattingre S, Smith GK*, et al.* (2012). Cathepsin D is partly endocytosed by the LRP1 receptor and inhibits LRP1-regulated intramembrane proteolysis. Oncogene 31**:** 3202-3212.

Diskin B, Adam S, Cassini MF, Sanchez G, Liria M, Aykut B*, et al.* (2020). PD-L1 engagement on T cells promotes self-tolerance and suppression of neighboring macrophages and effector T cells in cancer. Nat Immunol 21**:** 442-454.

Dong H, Diao H, Zhao Y, Xu H, Pei S, Gao J*, et al.* (2019). Overexpression of matrix metalloproteinase-9 in breast cancer cell lines remarkably increases the cell malignancy largely via activation of transforming growth factor beta/SMAD signalling. Cell Prolif 52**:** e12633.

Du H, Yi Z, Wang L, Li Z, Niu B, & Ren G (2020). The co-expression characteristics of LAG3 and PD-1 on the T cells of patients with breast cancer reveal a new therapeutic strategy. Int Immunopharmacol 78**:** 106113.

Emens LA, Adams S, Cimino-Mathews A, Disis ML, Gatti-Mays ME, Ho AY*, et al.* (2021). Society for Immunotherapy of Cancer (SITC) clinical practice guideline on immunotherapy for the treatment of breast cancer. J Immunother Cancer 9.

Fan Y, & He S (2022). The Characteristics of Tumor Microenvironment in Triple Negative Breast Cancer. Cancer Manag Res 14**:** 1-17.

Fang WB, Yao M, Brummer G, Acevedo D, Alhakamy N, Berkland C*, et al.* (2016). Targeted gene silencing of CCL2 inhibits triple negative breast cancer progression by blocking cancer stem cell renewal and M2 macrophage recruitment. Oncotarget 7**:** 49349-49367.

Fridman WH, Pages F, Sautes-Fridman C, & Galon J (2012). The immune contexture in human tumours: impact on clinical outcome. Nat Rev Cancer 12**:** 298-306.

Fusek M, & Vetvicka V (1994). Mitogenic function of human procathepsin D: the role of the propeptide. Biochem J 303 (Pt 3)**:** 775-780.

Glondu M, Liaudet-Coopman E, Derocq D, Platet N, Rochefort H, & Garcia M (2002). Down-regulation of cathepsin-D expression by antisense gene transfer inhibits tumor growth and experimental lung metastasis of human breast cancer cells. Oncogene 21**:** 5127-5134.

Gray MJ, Gong J, Hatch MM, Nguyen V, Hughes CC, Hutchins JT*, et al.* (2016). Phosphatidylserine-targeting antibodies augment the anti-tumorigenic activity of anti-PD-1 therapy by enhancing immune activation and downregulating pro-oncogenic factors induced by T-cell checkpoint inhibition in murine triple-negative breast cancers. Breast Cancer Res 18**:** 50.

Hasan L, Mazzucchelli L, Liebi M, Lis M, Hunger RE, Tester A*, et al.* (2006). Function of liver activation-regulated chemokine/CC chemokine ligand 20 is differently affected by cathepsin B and cathepsin D processing. J Immunol 176**:** 6512-6522.

Herroon MK, Rajagurubandara E, Rudy DL, Chalasani A, Hardaway AL, & Podgorski I (2013). Macrophage cathepsin K promotes prostate tumor progression in bone. Oncogene 32**:** 1580-1593.

Hoover RG, Gullickson G, & Kornbluth J (2012). Natural killer lytic-associated molecule plays a role in controlling tumor dissemination and metastasis. Front Immunol 3**:** 393.

Hu L, Roth JM, Brooks P, Luty J, & Karpatkin S (2008). Thrombin up-regulates cathepsin D which enhances angiogenesis, growth, and metastasis. Cancer Res 68**:** 4666-4673.

Huang L, Liu Z, Chen S, Liu Y, & Shao Z (2013). A prognostic model for triple-negative breast cancer patients based on node status, cathepsin-D and Ki-67 index. PLoS One 8**:** e83081.

Huang Y, Ma C, Zhang Q, Ye J, Wang F, Zhang Y*, et al.* (2015). CD4+ and CD8+ T cells have opposing roles in breast cancer progression and outcome. Oncotarget 6**:** 17462-17478.

Johnstone CN, Smith YE, Cao Y, Burrows AD, Cross RS, Ling X*, et al.* (2015). Functional and molecular characterisation of EO771.LMB tumours, a new C57BL/6-mouse-derived model of spontaneously metastatic mammary cancer. Dis Model Mech 8**:** 237-251.

Kang J, Yu Y, Jeong S, Lee H, Heo HJ, Park JJ*, et al.* (2020). Prognostic role of high cathepsin D expression in breast cancer: a systematic review and meta-analysis. Ther Adv Med Oncol 12**:** 1758835920927838.

Karkeni E, Morin SO, Bou Tayeh B, Goubard A, Josselin E, Castellano R*, et al.* (2019). Vitamin D Controls Tumor Growth and CD8+ T Cell Infiltration in Breast Cancer. Front Immunol 10**:** 1307.

Kasikara C, Davra V, Calianese D, Geng K, Spires TE, Quigley M*, et al.* (2019). Pan-TAM Tyrosine Kinase Inhibitor BMS-777607 Enhances Anti-PD-1 mAb Efficacy in a Murine Model of Triple-Negative Breast Cancer. Cancer Res 79**:** 2669-2683.

Ketscher A, Ketterer S, Dollwet-Mack S, Reif U, & Reinheckel T (2016). Neuroectoderm-specific deletion of cathepsin D in mice models human inherited neuronal ceroid lipofuscinosis type 10. Biochimie 122**:** 219-226.

Ketterer S, Mitschke J, Ketscher A, Schlimpert M, Reichardt W, Baeuerle N*, et al.* (2020). Cathepsin D deficiency in mammary epithelium transiently stalls breast cancer by interference with mTORC1 signaling. Nat Commun 11**:** 5133.

Khalkhali-Ellis Z, & Hendrix MJ (2014). Two Faces of Cathepsin D: Physiological Guardian Angel and Pathological Demon. Biol Med (Aligarh) 6.

Kyriazoglou A, Kaparelou M, Goumas G, Liontos M, Zakopoulou R, Zografos E*, et al.* (2022). Immunotherapy in HER2-Positive Breast Cancer: A Systematic Review. Breast Care (Basel) 17**:** 63-70.

Laurent-Matha V, Huesgen PF, Masson O, Derocq D, Prebois C, Gary-Bobo M*, et al.* (2012). Proteolysis of cystatin C by cathepsin D in the breast cancer microenvironment. FASEB J.

Le Naour A, Koffi Y, Diab M, Le Guennec D, Rouge S, Aldekwer S*, et al.* (2020). EO771, the first luminal B mammary cancer cell line from C57BL/6 mice. Cancer Cell Int 20**:** 328.

Lilley E, Stanford SC, Kendall DE, Alexander SPH, Cirino G, Docherty JR*, et al.* (2020). ARRIVE 2.0 and the British Journal of Pharmacology: Updated guidance for 2020. Br J Pharmacol 177**:** 3611-3616.

Liu J, Blake SJ, Yong MC, Harjunpaa H, Ngiow SF, Takeda K*, et al.* (2016). Improved Efficacy of Neoadjuvant Compared to Adjuvant Immunotherapy to Eradicate Metastatic Disease. Cancer Discov 6**:** 1382-1399.

Majidpoor J, & Mortezaee K (2021). The efficacy of PD-1/PD-L1 blockade in cold cancers and future perspectives. Clin Immunol 226**:** 108707.

Mansouri H, Alcaraz LB, Mollevi C, Mallavialle A, Jacot W, Boissiere-Michot F*, et al.* (2020). Co-Expression of Androgen Receptor and Cathepsin D Defines a Triple-Negative Breast Cancer Subgroup with Poorer Overall Survival. Cancers (Basel) 12.

Masson O, Bach AS, Derocq D, Prebois C, Laurent-Matha V, Pattingre S*, et al.* (2010). Pathophysiological functions of cathepsin D: Targeting its catalytic activity versus its protein binding activity? Biochimie 92**:** 1635-1643.

Maynadier M, Farnoud R, Lamy PJ, Laurent-Matha V, Garcia M, & Rochefort H (2013). Cathepsin D stimulates the activities of secreted plasminogen activators in the breast cancer acidic environment. Int J Oncol 43**:** 1683-1690.

Mihich E, & Ehrke MJ (2000). Anticancer drugs plus cytokines: immunodulation based therapies of mouse tumors. Int J Immunopharmacol 22**:** 1077-1081.

Mijanovic O, Petushkova AI, Brankovic A, Turk B, Solovieva AB, Nikitkina AI*, et al.* (2021). Cathepsin D-Managing the Delicate Balance. Pharmaceutics 13.

Munir MT, Kay MK, Kang MH, Rahman MM, Al-Harrasi A, Choudhury M*, et al.* (2021). Tumor-Associated Macrophages as Multifaceted Regulators of Breast Tumor Growth. Int J Mol Sci 22.

Park S, Jiang Z, Mortenson ED, Deng L, Radkevich-Brown O, Yang X*, et al.* (2010). The therapeutic effect of anti-HER2/neu antibody depends on both innate and adaptive immunity. Cancer Cell 18**:** 160-170.

Pelekanou V, Villarroel-Espindola F, Schalper KA, Pusztai L, & Rimm DL (2018). CD68, CD163, and matrix metalloproteinase 9 (MMP-9) co-localization in breast tumor microenvironment predicts survival differently in ER-positive and -negative cancers. Breast Cancer Res 20**:** 154.

Percie du Sert N, Hurst V, Ahluwalia A, Alam S, Avey MT, Baker M*, et al.* (2020). The ARRIVE guidelines 2.0: Updated guidelines for reporting animal research. Br J Pharmacol 177**:** 3617-3624.

Perez-Lanzon M, Carbonnier V, Cordier P, De Palma FDE, Petrazzuolo A, Klein C*, et al.* (2023). New hormone receptor-positive breast cancer mouse cell line mimicking the immune microenvironment of anti-PD-1 resistant mammary carcinoma. J Immunother Cancer 11.

Pranjol MZI, Gutowski NJ, Hannemann M, & Whatmore JL (2017). Cathepsin D non-proteolytically induces proliferation and migration in human omental microvascular endothelial cells via activation of the ERK1/2 and PI3K/AKT pathways. Biochim Biophys Acta 1865**:** 25-33.

Rovero S, Amici A, Di Carlo E, Bei R, Nanni P, Quaglino E*, et al.* (2000). DNA vaccination against rat her-2/Neu p185 more effectively inhibits carcinogenesis than transplantable carcinomas in transgenic BALB/c mice. J Immunol 165**:** 5133-5142.

Rye IH, Huse K, Josefsson SE, Kildal W, Danielsen HE, Schlichting E*, et al.* (2022). Breast cancer metastasis: immune profiling of lymph nodes reveals exhaustion of effector T cells and immunosuppression. Mol Oncol 16**:** 88-103.

Salmon H, Idoyaga J, Rahman A, Leboeuf M, Remark R, Jordan S*, et al.* (2016). Expansion and Activation of CD103(+) Dendritic Cell Progenitors at the Tumor Site Enhances Tumor Responses to Therapeutic PD-L1 and BRAF Inhibition. Immunity 44**:** 924-938.

Siintola E, Partanen S, Stromme P, Haapanen A, Haltia M, Maehlen J*, et al.* (2006). Cathepsin D deficiency underlies congenital human neuronal ceroid-lipofuscinosis. Brain 129**:** 1438-1445.

Souza-Fonseca-Guimaraes F (2016). NK cell-based immunotherapies: awakening the innate anti-cancer response. Discov Med 21**:** 197-203.

Sow HS, Benonisson H, Brouwers C, Linssen MM, Camps M, Breukel C*, et al.* (2020). Immunogenicity of rat-neu(+) mouse mammary tumours determines the T cell-dependent therapeutic efficacy of anti-neu monoclonal antibody treatment. Sci Rep 10**:** 3933.

Steel JC, Waldmann TA, & Morris JC (2012). Interleukin-15 biology and its therapeutic implications in cancer. Trends Pharmacol Sci 33**:** 35-41.

Tariq M, Zhang J, Liang G, Ding L, He Q, & Yang B (2017). Macrophage Polarization: Anti-Cancer Strategies to Target Tumor-Associated Macrophage in Breast Cancer. J Cell Biochem 118**:** 2484-2501.

Uchimiak K, Badowska-Kozakiewicz AM, Sobiborowicz-Sadowska A, & Deptala A (2022). Current State of Knowledge on the Immune Checkpoint Inhibitors in Triple-Negative Breast Cancer Treatment: Approaches, Efficacy, and Challenges. Clin Med Insights Oncol 16**:** 11795549221099869.

van de Bovenkamp FS, Hafkenscheid L, Rispens T, & Rombouts Y (2016). The Emerging Importance of IgG Fab Glycosylation in Immunity. J Immunol 196**:** 1435-1441.

Vetvicka V, Vetvickova J, Hilgert I, Voburka Z, & Fusek M (1997). Analysis of the interaction of procathepsin D activation peptide with breast cancer cells. Int J Cancer 73**:** 403-409.

Vignon F, Capony F, Chambon M, Freiss G, Garcia M, & Rochefort H (1986). Autocrine growth stimulation of the MCF 7 breast cancer cells by the estrogen-regulated 52 K protein. Endocrinology 118**:** 1537-1545.

Wang R, Jaw JJ, Stutzman NC, Zou Z, & Sun PD (2012). Natural killer cell-produced IFN-gamma and TNF-alpha induce target cell cytolysis through up-regulation of ICAM-1. J Leukoc Biol 91**:** 299-309.

Watanabe H, Numata K, Ito T, Takagi K, & Matsukawa A (2004). Innate immune response in Th1- and Th2-dominant mouse strains. Shock 22**:** 460-466.

Watanabe MA, Oda JM, Amarante MK, & Cesar Voltarelli J (2010). Regulatory T cells and breast cancer: implications for immunopathogenesis. Cancer Metastasis Rev 29**:** 569-579.

Wojtukiewicz MZ, Pogorzelska M, & Polityńska B (2022). Immunotherapy for triple negative breast cancer: the end of the beginning or the beginning of the end? Cancer Metastasis Rev 41**:** 465-469.

Wolf M, Clark-Lewis I, Buri C, Langen H, Lis M, & Mazzucchelli L (2003). Cathepsin D specifically cleaves the chemokines macrophage inflammatory protein-1 alpha, macrophage inflammatory protein-1 beta, and SLC that are expressed in human breast cancer. Am J Pathol 162**:** 1183-1190.

Yang WC, Hwang YS, Chen YY, Liu CL, Shen CN, Hong WH*, et al.* (2017). Interleukin-4 Supports the Suppressive Immune Responses Elicited by Regulatory T Cells. Front Immunol 8**:** 1508.

Zhang C, Zhang M, & Song S (2018). Cathepsin D enhances breast cancer invasion and metastasis through promoting hepsin ubiquitin-proteasome degradation. Cancer Lett 438**:** 105-115.

Zheng X, Fang Z, Liu X, Deng S, Zhou P, Wang X*, et al.* (2018). Increased vessel perfusion predicts the efficacy of immune checkpoint blockade. J Clin Invest 128**:** 2104-2115.

Zheng Y, Han L, Chen Z, Li Y, Zhou B, Hu R*, et al.* (2022). PD-L1(+)CD8(+) T cells enrichment in lung cancer exerted regulatory function and tumor-promoting tolerance. iScience 25**:** 103785.

LEGENDS TO FIGURES

Figure 1. CathD expression and secretion, binding of anti-CathD antibodies, and tumour growth and immunological profile in preclinical TNBC and HER2-amplified BC models.

(A) CathD expression and secretion in the E0771 and TUBO mouse BC cell lines. Whole cell extracts (lysate, 20 µg proteins) and 24-hour conditioned media in the presence of serum (SN, 40 µl) were immunoblotted with an anti-mouse CathD antibody (#AF1029). HSC70 was used as loading control. Similar results were obtained in 3 independent experiments. These data are exploratory.

(B) CathD expression in E0771 and TUBO cell-derived tumours. Whole cytosols (5 µg proteins) from four E0771 and four TUBO cell-derived tumours were immunoblotted with anti-mouse CathD (#AF1029) and anti-HSC70 (loading control) antibodies. N=4 mice for E0771 and TUBO cell-derived tumours. These data are exploratory.

(C) CathD expression and localization in E0771 and TUBO cell-derived tumours. E0771 and TUBO cell-derived tumour sections were incubated with the F1M1 anti-CathD antibody (green). Nuclei were stained with Hoechst 33342 (blue). Scale bar, 10 µm. N=5 mice par group for E0771 and TUBO tumours.

(D) Binding of F1 and F1M1 to CathD secreted from E0771 and TUBO cells. Sandwich ELISA in which secreted CathD from E0771 cell (left panel) or TUBO cell (right panel) supernatants was added to wells pre-coated with an anti-CathD polyclonal antibody (#AF1029) in the presence of increasing concentrations of F1 and F1M1 anti-CathD antibodies. Binding of F1 and F1M1 to secreted CathD was revealed with an anti-mouse $F(ab')_2$ HRP-conjugated antibody. Mean ± SD (n=3). The EC_{50} values are shown. Similar results were obtained in 5 independent experiments.

(E) CD45, F4/80, and CD3 immunostaining in E0771 cell-derived tumours. Representative images of CD45, F4/80 and CD3 immunostaining in E0771 tumour grafts from 5 mice. Left panels show immunostaining of the tumour stroma interface and right panels show staining in the tumour. Scale bars, 100 µm (left) and 50 µm (right).

(F) CD45, F4/80 and CD3 immunostaining in TUBO cell-derived tumours. Representative images of CD45, F4/80 and CD3 immunostaining in TUBO tumour grafts from 5 mice. Left panels show immunostaining of the tumour stroma interface, and right panels show immunostaining in the tumour. Scale bars, 100 µm (left) and 50 µm (right).

(G) Immunological profile of E0771 cell-derived tumours. The percentage of $CD45^+$ immune cells was quantified by FACS and expressed relative to all living cells in E0771 cell-derived tumours (n=10) (left panel). The percentage of myeloid (middle panel) and lymphoid (right panel) cell populations was quantified by FACS and expressed relative to all $CD45^+$ immune cells. TAM: $CD11b^+$ $F4/80^+$ cells; M2-TAM: $CD11b^+$ $F4/80^+$ $CD206^+$ cells; M1-TAM: $CD11b^+$ $F4/80^+$ $CD206^-$ $CD11c^+$ cells; cDC: F4/80-$CD3^-$ $Ly6G^-$ $Ly6C^-$ $NKp46^-$ $B220^-$ $CD11c^{+/hi}$ cells, including cDC2 ($CD8^-$ $CD11b^+$) and cDC1 ($CD8^+$ $CD11b^-$); neutrophils: $F4/80^-$ $CD3^-$ $CD11b^+$ $Ly6G^+$ $Ly6C^+$ cells; monocytes: $F4/80^-$ $CD3^-$ $CD11b^+$ $Ly6G^-$ $Ly6C^+$ cells; NK: $F4/80^-$ $CD3^-$ $Ly6G^-$ $Ly6C^-$ $CD11b^{lo/+}$ $NKp46^+$ cells; T: $F4/80^-$ $CD3^+$ cells, including $CD8^+$ T and $CD4^+$ T. Data are shown as means ± SEM of 10 mice.

(H) Immunological profile of TUBO cell-derived tumours. Immune cell populations in TUBO tumours (n=10) were analysed as described in panel G (n=10). Data are shown as means ± SEM of 10 mice.

Figure 2. Therapeutic effect of the F1 and F1M1 anti-CathD mouse IgG2a antibodies in immunocompetent C57BL/6 mice grafted with TNBC cell line E0771 and in immunocompetent BALB/c mice grafted with TUBO cells.

(A) Tumour growth in mice grafted with E0771 cells. At day 2 post-graft, C57BL/6 mice were treated with F1 (n=9), F1M1 (n=9), or C1.18.4 isotype control (CTRL; n=9) (15 mg/kg) was initiated (intraperitoneal injection three times per week for 33 days). All mice were sacrificed at day 33. Tumour volume (in mm^3) is shown as the mean ± SEM of 9 mice per group. *, $P<0.05$, significantly different as indicated. $P=0.005$ for F1 versus CTRL, $P=0.002$ for F1M1 versus CTRL (mixed-effects multiple linear regression test).

(B) Individual tumour growth curves in mice grafted with E0771 cells. Spider plots show the tumour growth of each mouse in each group: CTRL (n=9 mice, left panel), F1 (n=9 mice, middle panel) and F1M1 (n=9 mice, right panel).

(C) Mean tumour volume at day 33 in mice grafted with E0771 cells. n=9 for CTRL; n=9 for F1; n=9 for F1M1. Data are the mean ± SEM of 9 mice per group. *, $P<0.05$, significantly different as indicated. $P=0.0136$ for F1 versus CTRL, $P=0.0194$ for F1M1 versus CTRL (Mann-Whitney *t*-test);

(**D) Weight monitoring in mice grafted with E0771 cells.** n=9 for CTRL; n=9 for F1; n=9 for F1M1. Data are the mean ± SEM of 9 mice per group.

(E) Tumour growth in mice grafted with TUBO cells. At day 2 post-graft, BALB/c mice were treated with F1 (n=12), F1M1 (n=12), or C1.18.4 isotype control (CTRL; n=12) (15 mg/kg) by intraperitoneal injection three times per week for 19 days. All mice were sacrificed at day 19. Tumour volume (in mm^3) is shown as the mean ± SEM of 12 mice per group. $P=0.390$ for F1 versus CTRL; $P=0.383$ for F1M1 versus CTRL (mixed-effects multiple linear regression test).

(F) Individual tumour growth curves in mice grafted with TUBO cells. Spider plots show the individual tumour growth in each treatment group: CTRL (n=12), F1 (n=12), and F1M1 (n=12).

(G) Mean tumour volume at day 19 in mice grafted with TUBO cells. CTRL (n=12), F1 (n=12) and F1M1 (n=12). Data are the mean ± SEM of 12 mice per group. $P=0.3699$ for F1 versus CTRL; $P=0.4863$ for F1M1 versus CTRL (Mann-Whitney *t*-test);

(H) Weight monitoring in mice grafted with TUBO cells. CTRL (n=12), F1 (n=12), and F1M1 (n=12). Data are the mean ± SEM of 12 mice per group.

Figure 3. Anti-CathD antibody-based therapy rebalances TAM recruitment and activation in E0771 cell-derived tumours.

(A) TAM recruitment. The percentage of $F4/80^+$ $CD11b^+$ TAMs was quantified by FACS and expressed relative to all $CD45^+$ immune cells in the tumour (n=9 for CTRL; n=7 for F1; n=8 for F1M1); *, $P<0.05$, significantly different as indicated. $P= 0.0393$ for F1 versus CTRL, $P=0.0464$ for F1M1 versus C1.18.1

control (CTRL) (Mann-Whitney *t*-test); mean ± SEM of 9 mice for CTRL, 7 mice for F1, and 8 mice for F1M1.

(B) M2-TAM recruitment. The percentage of F4/80$^+$ CD11b$^+$ CD206$^+$ M2-TAMs (left panel) was quantified by FACS and expressed relative to all CD45$^+$ immune cells in the tumour (n=9 for CTRL; n=7 for F1; n=8 for F1M1). *, *P*<0.05, significantly different as indicated. *P*= 0.0311 for F1 versus CTRL, *P*=0.0111 for F1M1 versus CTRL (Mann-Whitney *t*-test); data are the mean ± SEM of 9 mice for CTRL, 7 mice for F1, and 8 mice for F1M1.

(C) M1-TAM recruitment and activation. The percentage of F4/80$^+$ CD11b$^+$ CD11c$^+$ CD206$^-$ M1-TAMs (left panel) was quantified by FACS and expressed relative to all CD45$^+$ immune cells in the tumour (n=9 for CTRL; n=7 for F1; n=8 for F1M1); *P*= 0.8371 for F1 versus CTRL, *P*=0.8148 for F1M1 versus CTRL (Mann-Whitney *t*-test); data are the mean ± SEM of 9 mice for CTRL, 7 mice for F1, and 8 mice for F1M1. The percentage of activated CD86$^+$ M1-TAMs (middle panel) was quantified by FACS and expressed relative to all M1-TAMs (n=9 for CTRL; n=7 for F1; n=8 for F1M1), *P*= 0.14 for F1 versus CTRL; *P*=0.0495 for F1M1 versus CTRL (Mann-Whitney *t*-test); mean ± SEM of 9 mice for CTRL, 7 mice for F1, and 8 mice for F1M1. *, *P*<0.05, significantly different as indicated.

(D) Quantification of *Ccl2*, *Ccr2*, *Il10* and *Mmp9* mRNA expression. Total RNA was extracted from E0771 cell-derived tumours at treatment end (day 33) and *Ccl2*, *Ccr2*, *Il10* and *Mmp9* expression levels were analysed by RT-qPCR. Data are the mean ± SEM relative to *Rps9* expression of 8 mice for CTRL, 5 mice for F1, and 7 mice for F1M1 (CTRL n=8; F1 n=5; F1M1 n=7). For *Ccl2*, *P*=0.0575 for F1 versus CTRL and *P*=0.0190 for F1M1 versus CTRL. For *Ccr2*, *P*=0.0016 for F1 versus CTRL and *P*=0.0185 for F1M1 versus CTRL. For *Il10*, *P*=0.0031 for F1 versus CTRL and *P*=0.0003 for F1M1 versus CTRL. For *Mmp9*, *P*=0.0031 for F1 versus CTRL and *P*=0.0003 for F1M1 versus CTRL (Mann-Whitney *t*-test). *, *P*<0.05, significantly different as indicated.

Figure 4. Anti-CathD antibody-based therapy triggers NK cell activation in E0771 cell-derived tumours.

(A) NK cell recruitment and activation. The percentage of NKp46^{+} NK cells was quantified by FACS and expressed relative to all CD45^{+} immune cells in the tumour (n=9 for CTRL; n=7 for F1; n=8 for F1M1) (left panel). *P*=0.3510 for F1 vs CTRL, *P*=0.8884 for F1M1 vs CTRL. The percentage of activated (CD16^{+}) NK cells was quantified by FACS and expressed relative to all NK cells in the tumour (n=9 for CTRL; n=7 for F1; n=8 for F1M1) (right panel). *, *P*<0.05, significantly different as indicated. *P*=0.0002 for F1 versus CTRL, *P*=0.0142 for F1M1 versus CTRL (Mann-Whitney *t*-test); data are the mean ± SEM of 9 mice for CTRL, 7 mice for F1, and 8 mice for F1M1.

(B) Quantification of *Il15* and *Tnf* mRNA expression. Total RNA was extracted from E0771 cell-derived tumours at treatment end (day 33), and *Il15* and *Tnf* were analyzed by RT-qPCR. Data are the mean ± SEM relative to *RPS9* expression 8 mice for CTRL, 5 mice for F1, and 7 mice for F1M1 (CTRL n=8; F1 n=5; F1M1 n=7). *, *P*<0.05, significantly different as indicated. For *Il15*, *P*=0.0109 for F1 versus CTRL and *P*=0.0939 for F1M1 versus CTRL. For *Tnf*, *P*=0.0295 for F1 versus CTRL and *P*=0.0003 for F1M1 versus CTRL (Mann-Whitney *t*-test).

Figure 5. Anti-CathD antibody-based therapy increases the mRNA expression of Fc receptors in E0771 cell-derived tumours.

Total RNA was extracted from E0771 cell-derived tumours at treatment end (day 33), and *Fcgr1, Fcgr2b, Fcgr3, Fcgr4* and *Fcgrt* mRNA levels were analysed by RT-qPCR. Data are the mean ± SEM relative to *Rps9* expression of 8 mice for CTRL, 5 mice for F1, and 7 mice for F1M1 (CTRL n=8; F1 n=5; F1M1 n=7). *, *P*<0.05, significantly different as indicated. For *Fcgr1*, *P*=0.0016 for F1 versus CTRL and *P*=0.0003 for F1M1 versus CTRL. For *Fcgr2b*, *P*=0.0016 for F1 versus CTRL and *P*=0.0003 for F1M1 versus CTRL. For *Fcgr3*, *P*=0.0016 for F1 versus CTRL and *P*=0.0003 for F1M1 versus CTRL. For *Fcgr4*, *P*=0.0016 for F1 versus CTRL and *P*=0.0003 for F1M1 versus CTRL. For *Fcgrt*, *P*=0.0016 for F1 versus CTRL and *P*=0.0003 for F1M1 versus CTRL (Mann-Whitney *t*-test).

Figure 6. Anti-CathD antibody-based therapy induces the recruitment and maturation of cDC1 cells in E0771 cell-derived tumours.

(A) cDC recruitment. The percentage of the cDC (left panel), cDC2 (middle panel) and cDC1 (right panel) subtypes was quantified by FACS and expressed relative to all $CD45^+$ immune cells in the tumour (n=9 for CTRL; n=7 for F1; n=8 for F1M1). *, $P<0.05$, significantly different as indicated. For $CD11c^{+/hi}$ cDC, $P=0.2991$ for F1 versus CTRL and; $P=0.5414$ for F1M1 versus CTRL. For $CD11c^{+/hi}$ $CD8^-$ $CD11b^+$ cDC2 cells, $P>0.9$ for F1 versus CTRL and $P=0.6058$ for F1M1 versus CTRL. For $CD11c^{+/hi}$ $CD8^+$ $CD11b^-$ cDC1 cells, $P=0.0164$ for F1 versus CTRL and $P=0.0055$ for F1M1 versus CTRL (Mann-Whitney *t*-test); data are the mean ± SEM of 9 mice for CTRL, 7 mice for F1, and 8 mice for F1M1.

(B) cDC1 cell activation. The percentage of activated $CD86^+$ cDC1 cells was quantified by FACS and expressed relative to all cDC1 cells in the tumour (n=9 for CTRL; n=7 for F1; n=8 for F1M1). *, $P<0.05$, significantly different as indicated. $P=0.0360$ for F1 versus CTRL, $P=0.0053$ for F1M1 versus CTRL (Mann-Whitney *t*-test); data are the mean ± SEM of 9 mice for CTRL, 7 mice for F1, and 8 mice for F1M1.

(C) Quantification of *H2d1*, *H2k1*, *B2m*, and *Il12p40* mRNA expression. Total RNA was extracted from E0771 cell-derived tumours at treatment end (day 33). The expression levels of *H2d1*, *H2k1*, *B2m*, and *Il12p40* were quantified by RT-qPCR. Data are the mean ± SEM relative to *Rps9* expression of 8 mice for CTRL, 5 mice for F1, and 7 mice for F1M1 (CTRL n=8; F1 n=5; F1M1 n=7). *, $P<0.05$, significantly different as indicated. For *H2d1*, $P=0.0016$ for F1 versus CTRL and $P=0.0003$ for F1M1 versus CTRL. For *H2k1*, $P=0.0016$ for F1 versus CTRL and $P=0.0003$ for F1M1 versus CTRL. For *B2m*, $P=0.0016$ for F1 versus CTRL and $P=0.0003$ for F1M1 versus CTRL. For *Il12p40*, $P=0.0870$ for F1 versus CTRL and $P=0.0022$ for F1M1 versus CTRL (Mann-Whitney *t*-test).

Figure 7. Anti-CathD antibody-based therapy reduces T-cell exhaustion in E0771 cell-derived tumours.

(A) Recruitment of $CD4^+$ T cell and PDL-1^+ $CD4^+$ T cells. The percentage of $CD4^+$ T cells was quantified by FACS and expressed relative to all $CD45^+$ immune cells in the tumour (left panel). *P*=0.9182 for F1 versus CTRL and *P*=0.6730 for F1M1 versus CTRL. The percentage of $PDL1^+$ $CD4^+$ T cells was quantified by FACS and expressed relative to all $CD4^+$ T cells in the tumour (right panel). *P*=0.0164 for F1 versus CTRL and *P*=0.0206 for F1M1 versus CTRL (Mann-Whitney *t*-test); data are the mean ± SEM of 9 mice for CTRL, 7 mice for F1, and 8 mice for F1M1. *, *P*<0.05, significantly different as indicated.

(B) Recruitment of $CD8^+$ T cells and PDL-1^+ $CD8^+$ T cells. The percentage of $CD8^+$ T cells was quantified by FACS and expressed relative to all $CD45^+$ immune cells in the tumour (left panel). *P*=0.6065 for F1 versus CTRL and *P*=0.4807 for F1M1 versus CTRL. The percentage of $PDL1^+$ $CD8^+$ T cells was quantified by FACS and expressed relative to all $CD8^+$ T cells in the tumour (right panel). *P*=0.0311 for F1 versus CTRL and *P*=0.036 for F1M1 versus CTRL (Mann-Whitney *t*-test); data are the mean ± SEM of 9 mice for CTRL, 7 mice for F1, and 8 mice for F1M1. *, *P*<0.05, significantly different as indicated.

(C) Quantification of *Lag3* and *Tigit* mRNA expression. Total RNA was extracted from E0771 cell-derived tumours at treatment end (day 33) and *Lag3* (left panel) and *Tigit* (right panel) were analysed by RT-qPCR. Data are the mean ± SEM relative to *Rps9* expression of 8 mice for CTRL, 5 mice for F1, and 7 mice for F1M1 (CTRL n=8; F1 n=5; F1M1 n=7). *, *P*<0.05, significantly different as indicated. For *Lag3*, *P*=0.0109 for F1 versus CTRL and *P*=0.0006 for F1M1 versus CTRL. For *Tigit*, *P*=0.0016 for F1 versus CTRL and *P*=0.0012 for F1M1 versus CTRL (Mann-Whitney *t*-test).

(D) Quantification of *Foxp3* and *IL4* mRNA expression. Total RNA was extracted and analysed by RT-qPCR. Data are the mean ± SEM relative to *Rps9* expression of 8 mice for CTRL, 5 mice for F1, and 7 mice for F1M1 (CTRL n=8; F1 n=5; F1M1 n=7). *, *P*<0.05, significantly different as indicated. For *Foxp3*, *P*=0.0016 for F1 versus CTRL and *P*=0.0129 for F1M1 versus CTRL. For *Il4*, *P*=0.0016 for F1 versus CTRL and *P*=0.0180 for F1M1 versus CTRL (Mann-Whitney *t*-test).

LEGEND TO SUPPLEMENTARY FIGURES AND TABLES.

Figure S1. CathD expression and secretion in the 4T1 murine TNBC cell line.

Whole cell extracts (lysate, 20 µg proteins) and 24-hour conditioned media (SN, 40 µl) were separated by 13.5% SDS-PAGE and immunoblotted with an anti-mouse CathD antibody (#AF1029). Similar results were obtained in 3 independent experiments. These data are exploratory.

Figure S2. Coomassie blue staining of the F1 and F1M1 mouse IgG2a antibodies.

The mouse IgG2a F1 and F1M1 (2.5 µg) antibodies were separated on 17% SDS-PAGE followed by Coomassie blue staining. CTRL, C1.18.4 isotype control. Similar results were obtained in 2 independent experiments. These data are exploratory.

Figure S3. Growth of E0771 and TUBO cell-derived tumours and comparison of their immunological profiles.

(A) Growth of E0771 cell-derived tumours. E0771 cells were injected in the mammary fat pad of C57BL/6 mice. Mice (n=10) were sacrificed at day 35. Tumour volume (in mm^3) is shown as the mean ± SEM of 10 mice.

(B) Growth of TUBO cell-derived tumours. TUBO cells were injected subcutaneously in BALB/c mice. Mice (n=10) were sacrificed at day 21. Tumour volume (in mm^3) is shown as the mean ± SEM of 10 mice.

(C) Comparison of the immunological profiles of E0771 and TUBO cell-derived tumours by immunophenotyping. The percentages of the myeloid (left panel) and lymphoid (right panel) cell populations were quantified by FACS and expressed relative to all living cells in E0771 cell-derived tumours (black bars) (n=10) and TUBO cell-derived tumours (grey bars) (n=10). TAM, $CD11b^+$ $F4/80^+$ cells; M2-TAM, $CD11b^+$ $F4/80^+$ $CD206^+$ cells; M1-TAM, $CD11b^+$ $F4/80^+$ $CD206^-$ $CD11c^+$ cells; cDC, F4/80- $CD3^-$ $Ly6G^-$ $Ly6C^-$ $NKp46^-$ $B220^-$ $CD11c^{+/hi}$ cells, including cDC2 ($CD8^-$ $CD11b^+$) and cDC1 ($CD8^+$ $CD11b^-$); neutrophils, $F4/80^-$ $CD3^-$ $CD11b^+$ $Ly6G^+$ $Ly6C^+$ cells; monocytes, $F4/80^-$ $CD3^-$ $CD11b^+$ $Ly6G^-$ $Ly6C^+$ cells;

NK, F4/80^{-} CD3^{-} Ly6G^{-} Ly6C^{-} CD11b$^{-/lo}$ NKp46^{+} cells; T, F4/80^{-} CD3^{+} cells, including CD8^{+} T and CD4^{+} T cells. Data are shown as the mean ± SEM of 10 mice.

Figure S4. Schematic representation of the gating procedure to isolate immune populations in E0771 tumours by flow cytometry. Selected populations are indicated in red.

Figure S5. Schematic representation of the gating procedure to isolate immune populations in TUBO tumours by flow cytometry. Selected populations are indicated in red.

Figure S6. Randomization of immunocompetent C57BL/6 mice grafted with E0771 cells.
E0771 cells were injected in the mammary fat pad of C57BL/6 mice. At day 2 post-graft, E0771 cell bioluminescence was quantified to distribute mice in three groups with comparable luminescence to be treated with F1 (n=9), F1M1 (n=9), or C1.18.4 isotype control (CTRL; n=9). Bioluminescence data are the mean ± SEM of 9 mice per group.

Figure S7. Schematic representation of the gating procedure to isolate immune populations in PBLs (A) and in dLNs (B) from mice grafted with E0771 cancer cells. Selected populations are indicated in red.

Figure S8. Anti-CathD antibody-based therapy does not affect the proportion of neutrophils in PBLs from mice grafted with E0771 cancer cells. The percentage of neutrophils was quantified by FACS at day 33 and expressed relative to all CD45^{+} immune cells in PBL samples (n=9 for C1.18.4 CTRL; n=7 for F1; n=8 for F1M1). Data are the mean ± SEM of 9 mice for CTRL, 7 mice for F1, and 8 mice for F1M1. *P*=0.7577 pour F1 versus CTRL; *P*=0.4807 for F1M1 versus CTRL.

Figure S9. Schematic representation of the gating procedure to isolate immune populations in PBLs (A) and in dLNs (B) from mice grafted with TUBO cancer cells. Selected populations are indicated in red.

Figure S10. Anti-CathD antibody-based therapy does not affect the proportion of neutrophils in PBLs from mice grafted with TUBO cancer cells. The percentage of neutrophils was quantified by FACS at day 19 and expressed relative to all $CD45^+$ immune cells in PBL samples (n=12 for C1.18.4 CTRL; n=12 for F1; n=12 for F1M1). Data are the mean ± SEM of 12 mice for CTRL, 12 mice for F1, and 12 mice for F1M1. *P*=0.5411 pour F1 versus CTRL; *P*=0.2978 for F1M1 versus CTRL.

Figure S11. Anti-CathD antibody-based therapy triggers antitumour immunity in TUBO cell-derived tumours.

(A) TAM recruitment. The percentage of TAMs (left panel), M2-TAMs (middle panel) and M1-TAMs (right panel) was quantified by FACS and expressed relative to all $CD45^+$ immune cells in the tumour (n=11 for C1.18.4 CTRL, n=12 for F1, n=12 for F1M1). Data are the mean ± SEM of 12 mice for CTRL, 12 mice for F1, and 12 mice for F1M1. *, *P*<0.05, significantly different as indicated. For $F4/80^+$ $CD11b^+$ TAM, *P*= 0.0003 for F1 versus CTRL and *P*=0.0001 for F1M1 versus CTRL. For $F4/80^+$ $CD11b^+$ $CD206^+$ M2-TAMs, *P*=0.007 for F1 versus CTRL and P=0.009 for F1M1 versus CTRL. For $F4/80^+$ $CD11b^+$ $CD206^-$ $CD11^{c+}$ M1-TAMs, *P*=0.6178 for F1 versus CTRL and *P*=0.1175 for F1M1 versus CTRL (Mann-Whitney *t*-test).

(B) NK cell recruitment and activation. The percentage of $NKp46^+$ NK cells was quantified by FACS and expressed relative to all $CD45^+$ immune cells in the tumour (n=11 for C1.18.4 CTRL; n=12 for F1; n=12 for F1M1) (left panel). *P*=0.0225 for F1 versus CTRL; *P*=0.0512 for F1M1 versus CTRL. The percentage of activated $CD16^+$ NK cells was quantified by FACS and expressed relative to all NK cells in the tumour (n=11 for CTRL; n=12 for F1; n=12 for F1M1) (right panel). *, *P*<0.05, significantly different as indicated.

P=0.0317 for F1 versus CTRL and *P* <0.0001 for F1M1 versus CTRL (Mann-Whitney *t*-test); data are the mean ± SEM of 11 mice for CTRL, 12 mice for F1, and 12 mice for F1M1.

(C) cDC recruitment. The percentage of the cDC (left panel), cDC2 (middle panel) and cDC1 (right panel) subtypes was quantified by FACS and expressed relative to all $CD45^+$ immune cells in the tumour (n=11 for C1.18.4 CTRL; n=12 for F1; n=12 for F1M1). Data are the mean ± SEM of 11 mice for C1.18.4 CTRL, 12 mice for F1, and 12 mice for F1M1. *, *P*<0.05, significantly different as indicated. For $CD11c^+/^{hi}$ cDC, *P*=0.0084 for F1 versus CTRL and *P*=0.0055 for F1M1 versus CTRL. For $CD11c^+/^{hi}$ $CD8^-$ $CD11b^+$ cDC2 cells, *P*=0.0256 for F1 versus CTRL and *P* <0.0001 for F1M1 versus CTRL. For $CD11c^+/^{hi}$ $CD8^+$ $CD11b^-$ cDC1 cells, *P*=0.0007 for F1 versus CTRL and *P*=0.0016 for F1M1 versus CTRL (Mann-Whitney *t*-test).

(D) cDC1 cell activation. The percentage of activated $CD86^+$ cDC1 cells was quantified by FACS and expressed relative to all cDC1 cells in the tumour (n=11 for C1.18.4 CTRL; n=12 for F1; n=12 for F1M1). *P*=0.0083 for F1 versus CTRL, *P* <0.0001 for F1M1 versus CTRL (Mann-Whitney *t*-test); data are the mean ± SEM of 11 mice for CTRL, 12 mice for F1, and 12 mice for F1M1. *, *P*<0.05, significantly different as indicated.

Figure S12. Anti-CathD antibody-based therapy does not affect NK cell activation in PBLs from mice grafted with E0771 TNBC cells.

The percentage of $NKp46^+$ NK cells was quantified by FACS and expressed relative to all $CD45^+$ immune cells in PBL samples (n=9 for C1.18.4 CTRL; n=7 for F1; n=8 for F1M1) (left panel). *P*=0.9182 for F1 versus CTRL, *P*=0.3337 for F1M1 versus CTRL. The percentage of activated $CD16^+$ NK cells was quantified by FACS and expressed relative to all NK cells in PBL samples (n=9 for C1.18.4 CTRL; n=7 for F1; n=8 for F1M1) (right panel). *P*=0.3510 for F1 versus CTRL, *P*=0.9626 for F1M1 versus CTRL (Mann-Whitney *t*-test); data are the mean ± SEM of 9 mice for CTRL, 7 mice for F1, and 8 mice for F1M1.

Figure S13. Anti-CathD antibody-based therapy increases the percentage of $CD86^+$ antigen-presenting B cells in E0771 cell-derived tumours.

The percentage of $B220^+$ B cells was quantified by FACS and expressed relative to all $CD45^+$ immune cells in the tumour (n=9 for CTRL; n=7 for F1; n=8 for F1M1) (left panel). *P*=0.4698 for F1 versus CTRL, *P*=0.8884 for F1M1 versus CTRL. The percentage of $CD86^+$ $B220^+$ B cells was quantified by FACS and expressed relative to all B cells in the tumour (n=9 for CTRL; n=7 for F1; n=8 for F1M1) (right panel). *, *P*<0.05, significantly different as indicated. *P*=0.0418 for F1 versus CTRL, *P*=0.0152 for F1M1 versus CTRL (Mann-Whitney *t*-test); data are the mean ± SEM of 9 mice for CTRL, 7 mice for F1, and 8 mice for F1M1.

Figure S14. Effect of anti-CathD antibody-based therapy on PD-1^+ T cell recruitment in E0771 cell-derived tumours.

(A) Recruitment of PD-1^+ $CD4^+$ T cells. The percentage of PD-1^+ $CD4^+$ T cells was quantified by FACS and expressed relative to all $CD4^+$ T cells in the tumour (n=9 for CTRL; n=7 for F1; n=8 for F1M1). *P*=0.7577 for F1 versus CTRL and *P*=0.5414 for F1M1 versus CTRL (Mann-Whitney *t*-test); data are the mean ± SEM of 9 mice for CTRL, 7 mice for F1, and 8 mice for F1M1.

(B) Recruitment of PD-1^+ $CD8^+$ T cells. The percentage of PD-1^+ $CD8^+$ T cells was quantified by FACS and expressed relative to all $CD8^+$ T cells in the tumour (n=9 for CTRL; n=7 for F1; n=8 for F1M1). *P*=0.2523 for F1 versus CTRL and *P*=0.5580 for F1M1 versus CTRL (Mann-Whitney *t*-test); data are the mean ± SEM of 9 mice for CTRL, 7 mice for F1, and 8 mice for F1M1.

Figure S15. Anti-CathD antibody-based therapy reduces T-cell exhaustion in dLNs but not in PBLs from mice grafted with E0771 TNBC cells.

(A) Recruitment of $CD4^+$, PDL-1^+ $CD4^+$, and $LAG3^+$ $CD4^+$ T cells in dLNs. The percentage of $CD4^+$ T cells was quantified by FACS and expressed relative to all $CD45^+$ immune cells in the dLNs (left panel). *P*=0.4079 for F1 versus CTRL, *P*=0.1912 for F1M1 versus CTRL. The percentage of $PDL1^+$ $CD4^+$ T cells was quantified by FACS and expressed relative to all $CD45^+$ T cells in the dLNs (middle panel). Data are the mean ± SEM of 9 mice for CTRL, 7 mice for F1, and 8 mice for F1M1. *, *P*<0.05, significantly

different as indicated. *P*=0.0418 for F1 versus CTRL, *P*=0.1996 for F1M1 versus CTRL. The percentage of LAG3$^+$ CD4$^+$ T cells was quantified by FACS and expressed relative to all CD45$^+$ T cells in the dLNs (right panel). *P*=0.0873 for F1 versus CTRL, *P*=0.1919 for F1M1 versus CTRL (Mann-Whitney *t*-test).

(B) Recruitment of CD8$^+$, PDL-1$^+$ CD8$^+$, and LAG3$^+$ CD8$^+$ T cells in dLNs. The percentage of CD8$^+$ T cells was quantified by FACS and expressed relative to all CD45$^+$ immune cells in the dLNs (left panel). *P*=0.3510 for F1 versus CTRL, *P*=0.3842 for F1M1 versus CTRL. The percentage of PDL1$^+$ CD8$^+$ T cells was quantified by FACS and expressed relative to all CD45$^+$ T cells in the dLNs (middle panel). *P*=0.0115 for F1 versus CTRL, *P*=0.0274 for F1M1 versus CTRL. The percentage of LAG3$^+$ CD8$^+$ T cells was quantified by FACS and expressed relative to all CD45$^+$ T cells in the dLNs (right panel). *P*=0.0079 for F1 versus CTRL, *P*=0.0219 for F1M1 versus CTRL (Mann-Whitney *t*-test); data are the mean ± SEM (for CTRL, n=9 mice; for F1, n=7 mice; for F1M1, n=8 mice). *, *P*<0.05, significantly different as indicated.

(C) Recruitment of CD4$^+$, PDL-1$^+$ CD4$^+$, and LAG3$^+$ CD4$^+$ T cells in PBLs. The percentage of CD4$^+$ T cells was quantified by FACS and expressed relative to all CD45$^+$ immune cells in PBLs (left panel). *P*=0.4079 for F1 versus CTRL, *P*=0.5414 for F1M1 versus CTRL. The percentage of PDL1$^+$ CD4$^+$ T cells was quantified by FACS and expressed relative to all CD45$^+$ T cells in PBLs (middle panel). *P*=0.8371 for F1 versus CTRL, *P*=0.8340 for F1M1 versus CTRL. The percentage of LAG3$^+$ CD4$^+$ T cells was quantified by FACS and expressed relative to all CD45$^+$ T cells in PBLs (right panel). *P*=0.1341 for F1 versus CTRL, *P*=0.0192 for F1M1 versus CTRL (Mann-Whitney *t*-test); data are the mean ± SEM (for CTRL, n=9 mice; for F1, n=7 mice; for F1M1, n=8 mice). *, *P*<0.05, significantly different as indicated.

(D) Recruitment of CD8$^+$, PDL-1$^+$ CD8$^+$, and LAG3$^+$ CD8$^+$ T cells in PBLs. The percentage of CD8$^+$ T cells was quantified by FACS and expressed relative to all CD45$^+$ immune cells in PBLs (left panel). *P*=0.0445 for F1 versus CTRL, *P*=0.1075 for F1M1 versus CTRL. The percentage of PDL1$^+$ CD8$^+$ T cells was quantified by FACS and expressed relative to all CD45$^+$ T cells in PBLs (middle panel). *P*=0.8371 for F1 versus CTRL, *P*=0.3704 for F1M1 versus CTRL. The percentage of LAG3$^+$ CD8$^+$ T cells was quantified by FACS and expressed relative to all CD45$^+$ T cells in PBLs (right panel). *P*=0.3122 for F1 versus CTRL,

P=0.1593 for F1M1 versus CTRL (Mann-Whitney *t*-test); data are the mean ± SEM (for CTRL, n=9 mice; for F1, n=7 mice; for F1M1, n=8 mice). *, *P*<0.05, significantly different as indicated.

Figure S16. Anti-CathD antibody-based therapy reduces T-cell exhaustion in dLNs from mice grafted with TUBO cancer cells.

(A) Recruitment of $CD4^+$, $PDL\text{-}1^+$ $CD4^+$, and $LAG3^+$ $CD4^+$ T cells in tumour-dLNs. The percentage of $CD4^+$ T cells was quantified by FACS and expressed relative to all $CD45^+$ immune cells in tumour-dLNs (left panel). *P*=0.3546 for F1 versus CTRL, *P*=0.1135 for F1M1 versus CTRL. The percentage of $PDL1^+$ $CD4^+$ T cells was quantified by FACS and expressed relative to all $CD45^+$ T cells in tumour-dLNs (middle panel). *P*=0.0138 for F1 versus CTRL, *P*=0.0115 for F1M1 versus CTRL. The percentage of $LAG3^+$ $CD4^+$ T cells was quantified by FACS and expressed relative to all $CD45^+$ T cells in tumour-dLN (right panel). *P*=0.0614 for F1 versus CTRL; *P*=0.6169 for F1M1 versus CTRL (Mann-Whitney *t*-test); data are the mean ± SEM (for CTRL, n=11 mice; for F1, n=12 mice; for F1M1, n=12 mice). *, *P*<0.05, significantly different as indicated.

(B) Recruitment of $CD8^+$, $PDL\text{-}1^+$ $CD8^+$, and $LAG3^+$ $CD8^+$ T cells in tumour-dLNs. The percentage of $CD8^+$ T cells was quantified by FACS and expressed relative to all $CD45^+$ immune cells in tumour-dLNs (left panel). *P*=0.0613 for F1 versus CTRL, *P*=0.7013 for F1M1 versus CTRL. The percentage of $PDL1^+$ $CD8^+$ T cells was quantified by FACS and expressed relative to all $CD45^+$ T cells in tumour-dLNs (middle panel). *P*=0.0754 for F1 versus CTRL, *P*=0.01 for F1M1 versus CTRL. The percentage of $LAG3^+$ $CD8^+$ T cells was quantified by FACS and expressed relative to all $CD45^+$ T cells in tumour-dLNs (right panel). *P*=0.0205 for F1 versus CTRL, *P*=0.0242 for F1M1 versus CTRL (Mann-Whitney *t*-test); data are the mean ± SEM (for CTRL, n=11 mice; for F1, n=12 mice; for F1M1, n=12 mice). *, *P*<0.05, significantly different as indicated.

Table S1. Sequences of the primers used for RT-qPCR.

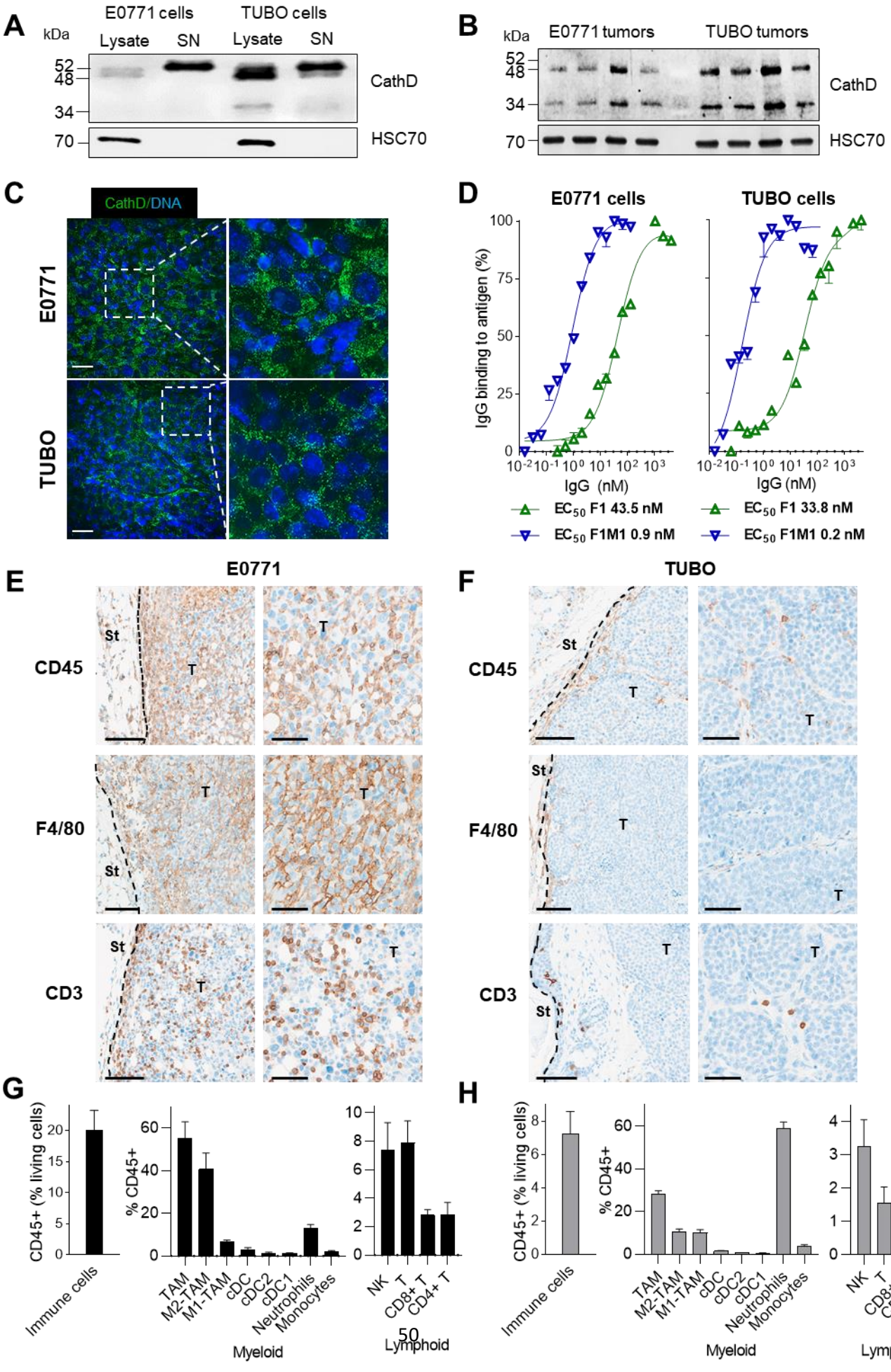
A
E0771 cells
TUBO cells
kDa
Lysate
SN
Lysate
SN
52
48
34
70
CathD
HSC70
B
kDa
E0771 tumors
TUBO tumors
52
48
34
70
CathD
HSC70
C
CathD/DNA
E0771
TUBO
D
E0771 cells
TUBO cells
IgG binding to antigen (%)
IgG (nM)
EC50 F1 43.5 nM
EC50 F1M1 0.9 nM
EC50 F1 33.8 nM
EC50 F1M1 0.2 nM
E
E0771
CD45
F4/80
CD3
St
T
F
TUBO
CD45
F4/80
CD3
St
T
G
CD45+ (% living cells)
% CD45+
Immune cells
TAM
M2-TAM
M1-TAM
cDC
cDC2
cDC1
Neutrophils
Monocytes
NK
T
CD8+ T
CD4+ T
Myeloid
Lymphoid
H
CD45+ (% living cells)
% CD45+
Immune cells
TAM
M2-TAM
M1-TAM
cDC
cDC2
cDC1
Neutrophils
Monocytes
NK
T
CD8+ T
CD4+ T
Myeloid
Lymphoid

Figure 1

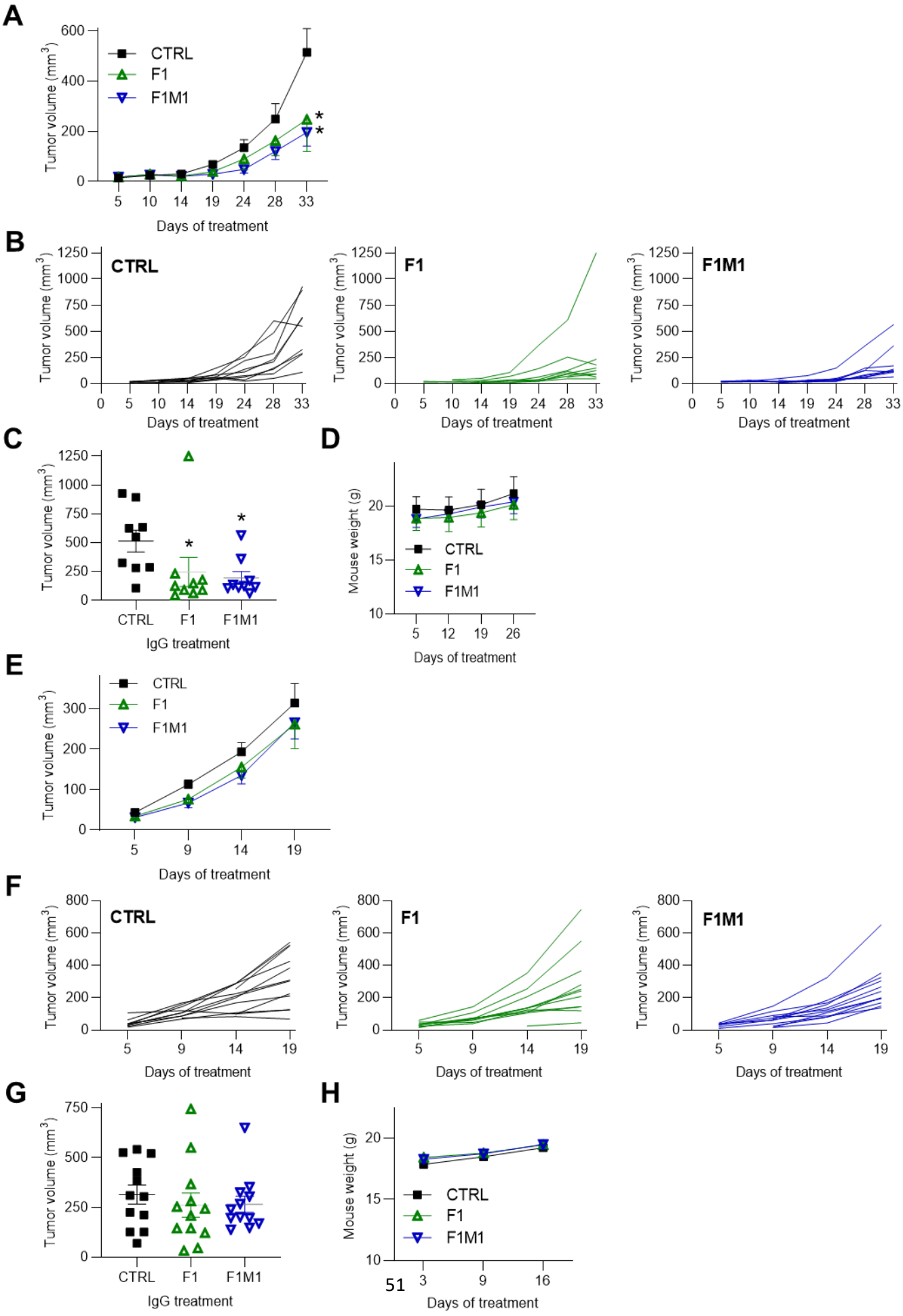
A
Tumor volume (mm3)
CTRL
F1
F1M1
Days of treatment
B
CTRL
F1
F1M1
C
IgG treatment
D
Mouse weight (g)
E
F
G
H

Figure 2

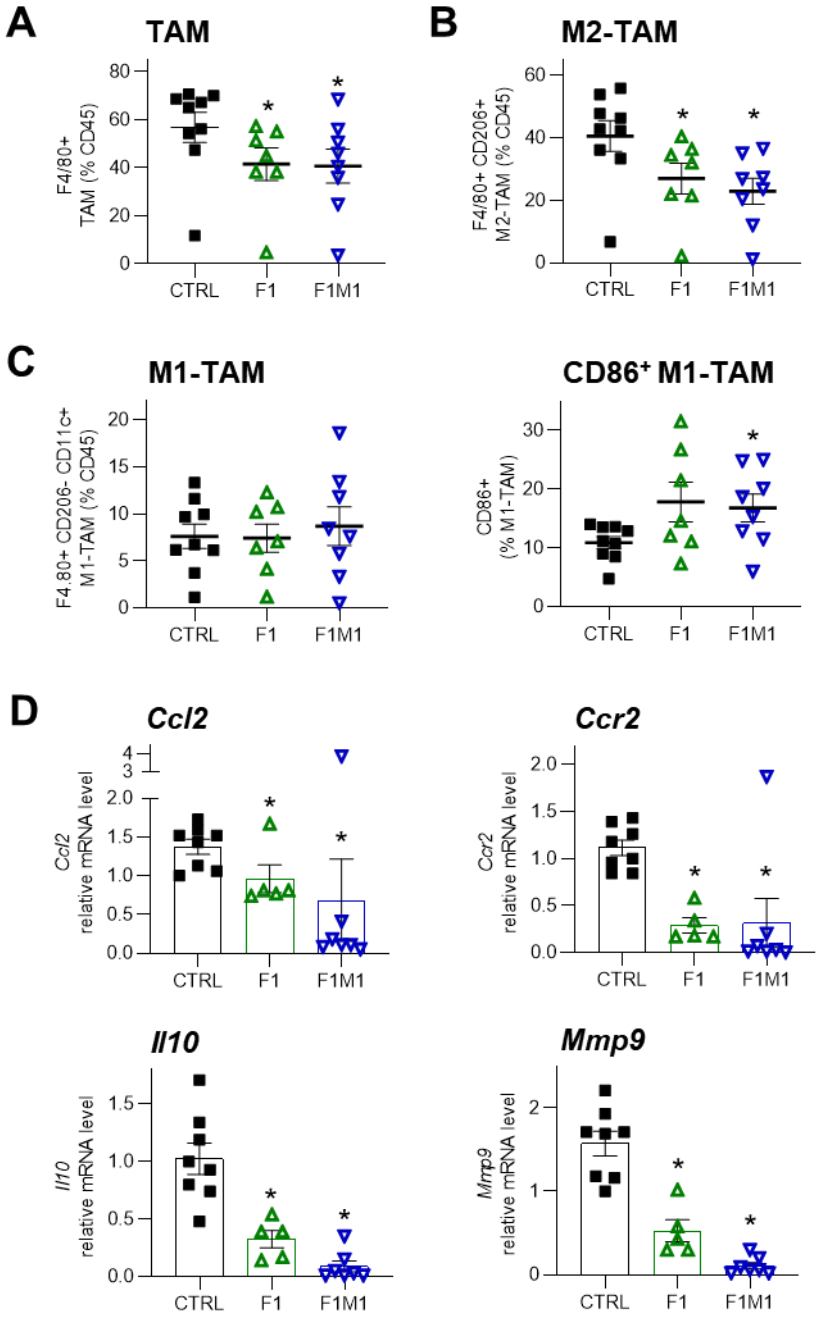
A
TAM
F4/80+ TAM (% CD45)
CTRL
F1
F1M1
B
M2-TAM
F4/80+ CD206+ M2-TAM (% CD45)
C
M1-TAM
F4.80+ CD206- CD11c+ M1-TAM (% CD45)
CD86+ M1-TAM
CD86+ (% M1-TAM)
D
Ccl2
Ccl2 relative mRNA level
Ccr2
Ccr2 relative mRNA level
Il10
Il10 relative mRNA level
Mmp9
Mmp9 relative mRNA level

Figure 3.

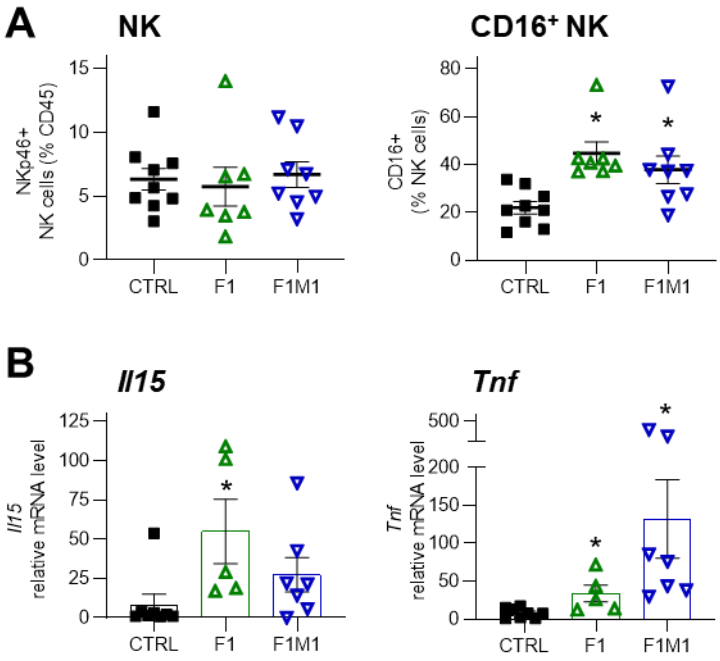
A
NK
NKp46+
NK cells (% CD45)
15
10
5
0
CTRL
F1
F1M1
CD16+ NK
CD16+
(% NK cells)
80
60
40
20
0
CTRL
F1
F1M1
B
Il15
Il15
relative mRNA level
125
100
75
50
25
0
CTRL
F1
F1M1
Tnf
Tnf
relative mRNA level
500
200
150
100
50
0
CTRL
F1
F1M1

Figure 4.

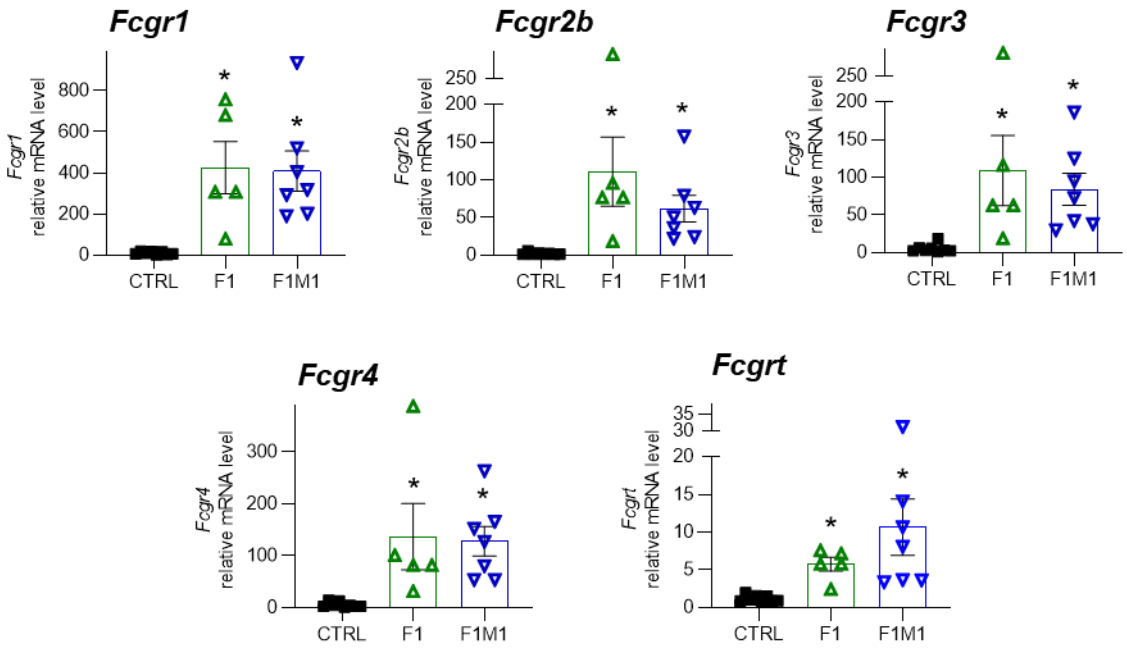
Fcgr1
Fcgr1 relative mRNA level
0
200
400
600
800
CTRL
F1
F1M1
Fcgr2b
Fcgr2b relative mRNA level
0
50
100
150
200
250
CTRL
F1
F1M1
Fcgr3
Fcgr3 relative mRNA level
0
50
100
150
200
250
CTRL
F1
F1M1
Fcgr4
Fcgr4 relative mRNA level
0
100
200
300
CTRL
F1
F1M1
Fcgrt
Fcgrt relative mRNA level
0
5
10
15
20
30
35
CTRL
F1
F1M1

Figure 5.

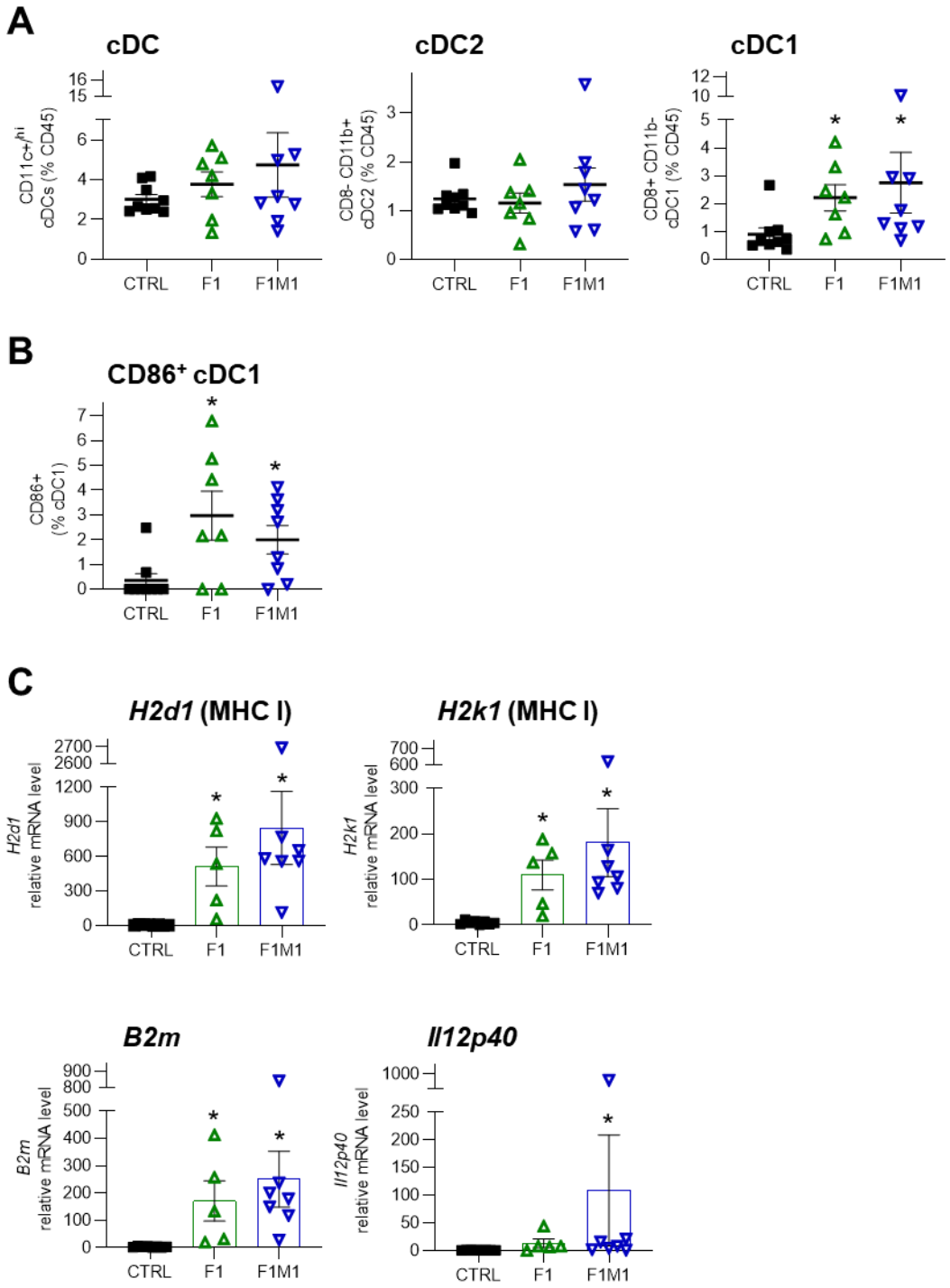
A
cDC
cDC2
cDC1
CD11c+hi cDCs (% CD45)
CD8- CD11b+ cDC2 (% CD45)
CD8+ CD11b- cDC1 (% CD45)
CTRL
F1
F1M1
B
CD86+ cDC1
CD86+ (% cDC1)
C
H2d1 (MHC I)
H2k1 (MHC I)
B2m
Il12p40
H2d1 relative mRNA level
H2k1 relative mRNA level
B2m relative mRNA level
Il12p40 relative mRNA level

Figure 6.

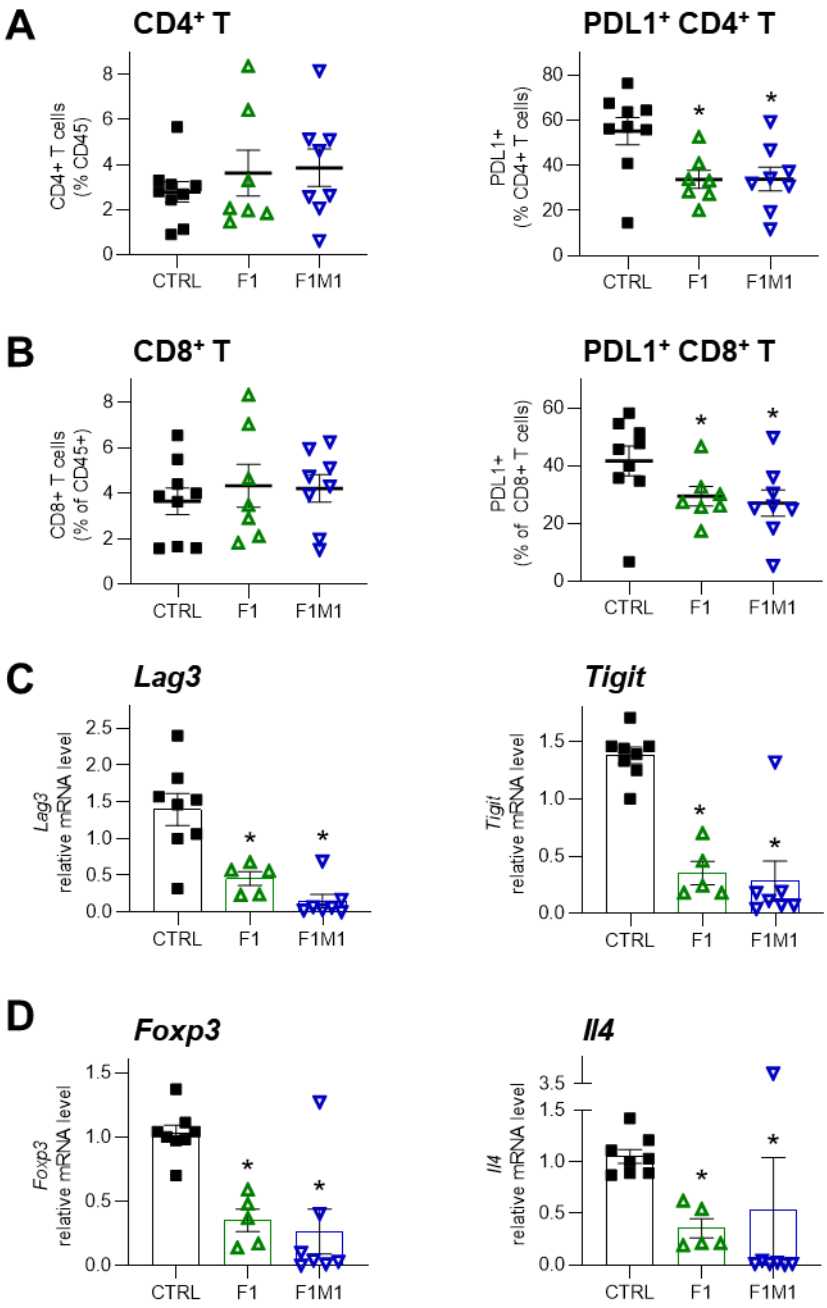
A
CD4⁺ T
CD4+ T cells (% CD45)
CTRL
F1
F1M1
PDL1⁺ CD4⁺ T
PDL1+ (% CD4+ T cells)
B
CD8⁺ T
CD8+ T cells (% of CD45+)
PDL1⁺ CD8⁺ T
PDL1+ (% of CD8+ T cells)
C
Lag3
Lag3 relative mRNA level
Tigit
Tigit relative mRNA level
D
Foxp3
Foxp3 relative mRNA level
Il4
Il4 relative mRNA level

Figure 7.

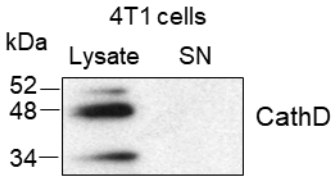

Figure S1. CathD expression and secretion in the 4T1 murine TNBC cell line.

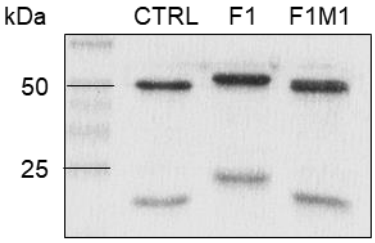

Figure S2. Coomassie blue staining of the F1 and F1M1 mouse IgG2a antibodies.

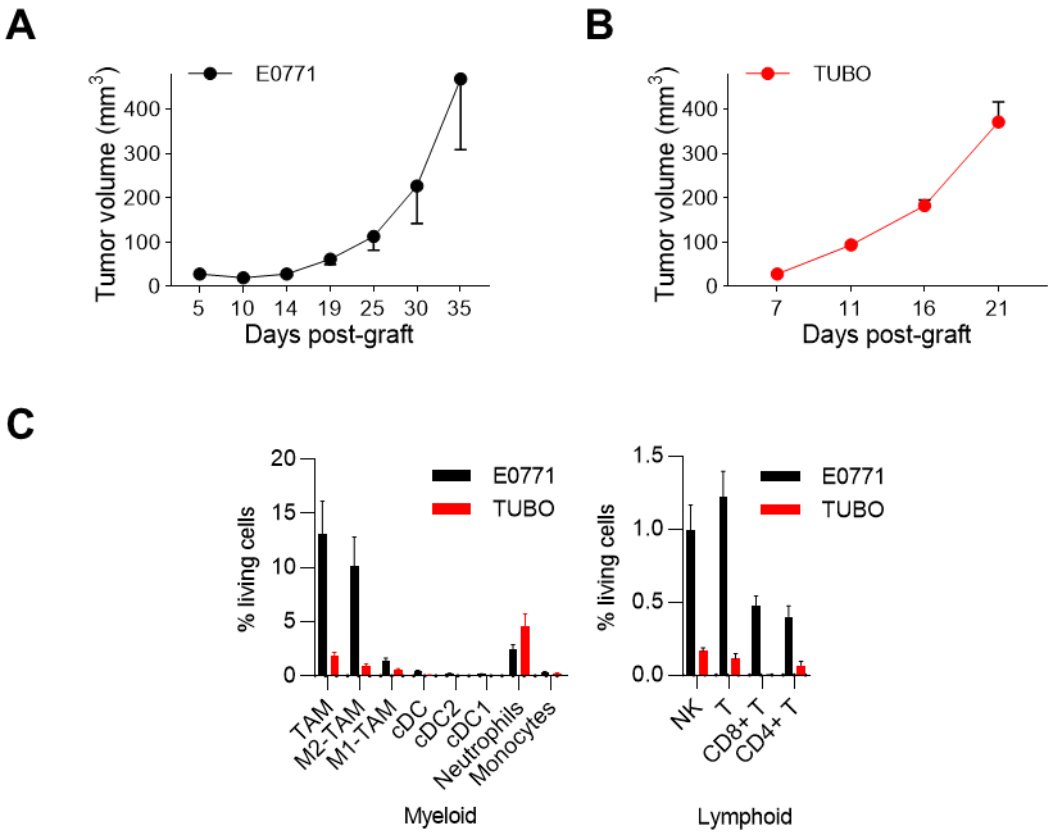

Figure S3. Growth of E0771 and TUBO cell-derived tumors and comparison of their immunological profiles.

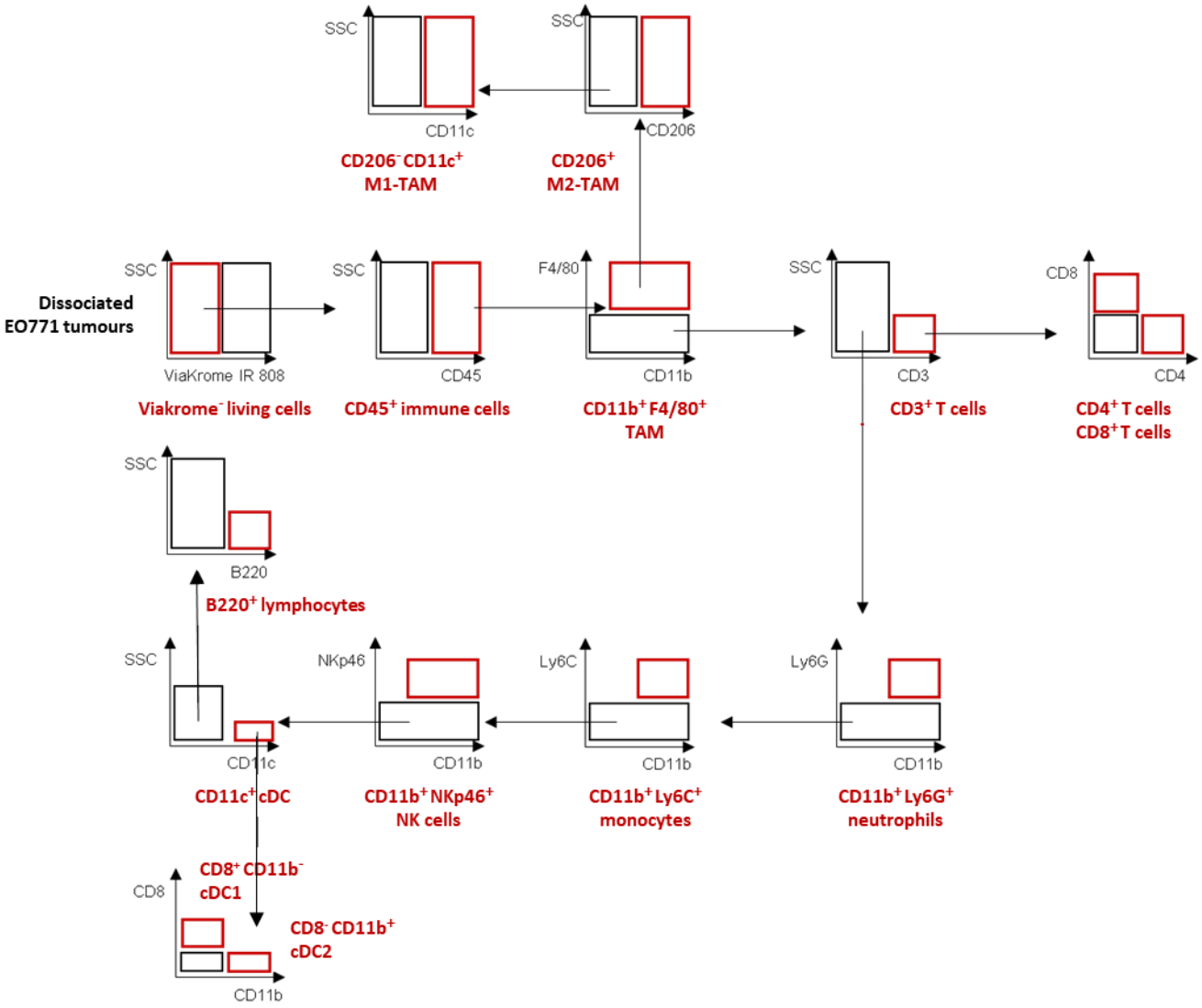

Figure S4. Schematic representation of the gating procedure to isolate immune populations in E0771 tumours by flow cytometry.

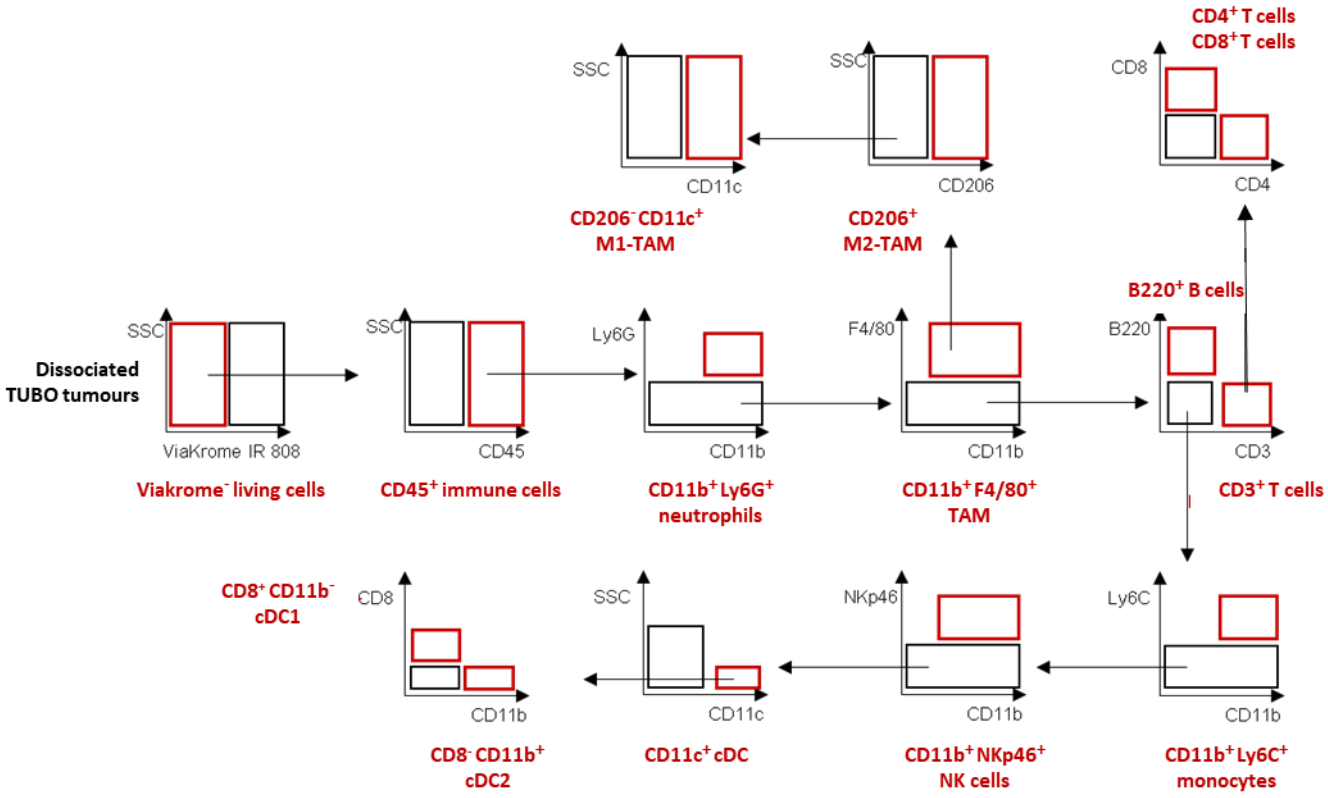

Figure S5. Schematic representation of the gating procedure to isolate immune populations in TUBO tumours by flow cytometry.

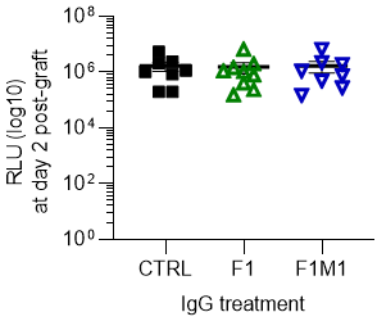

Figure S6. Randomization of immunocompetent C57BL/6 mice grafted with E0771 cells.

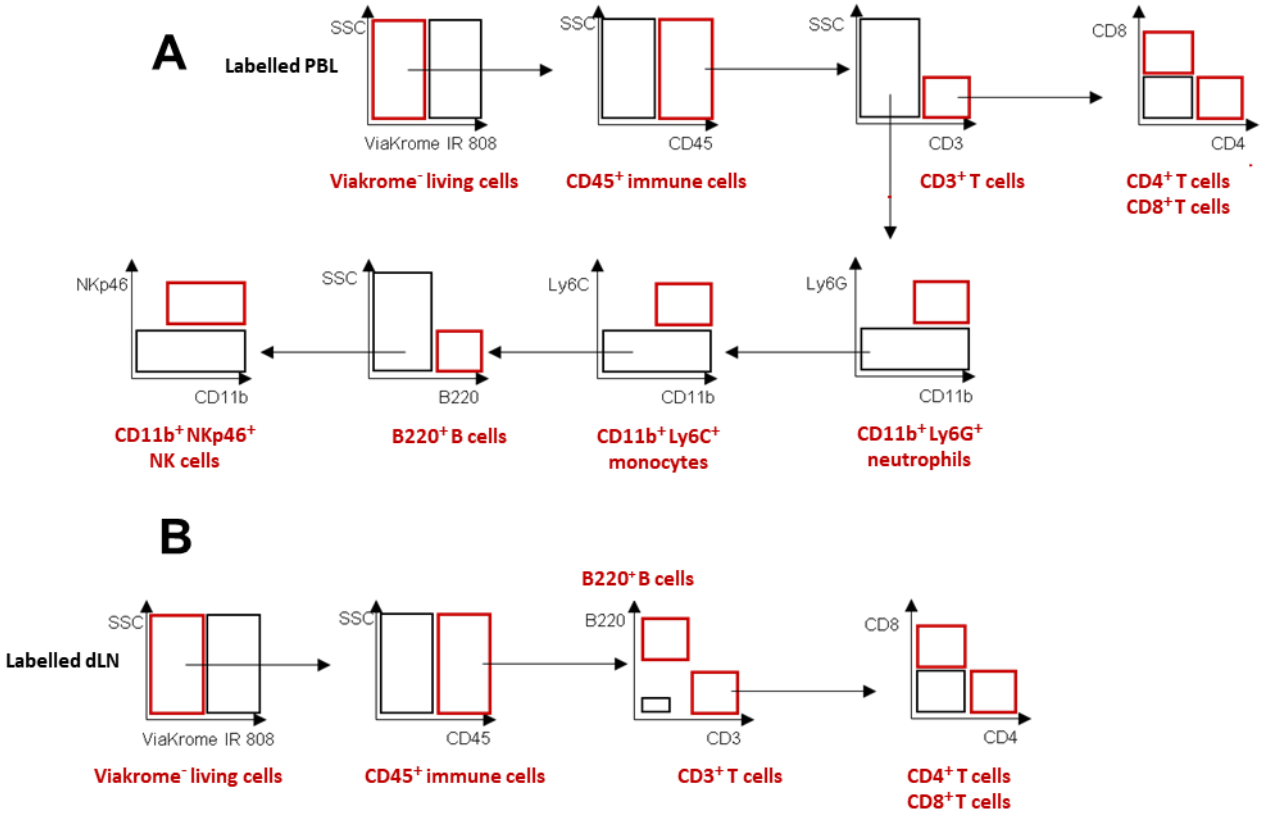

Figure S7. Schematic representation of the gating procedure to isolate immune populations in PBLs (A) and in dLNs (B) from mice grafted with E0771 cancer cells.

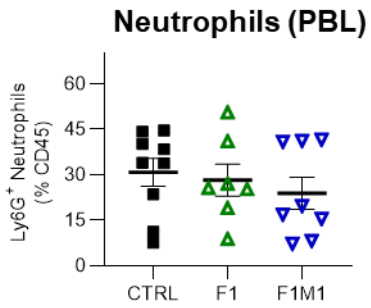

Figure S8. Anti-CathD antibody-based therapy does not affect the proportion of neutrophils in PBLs from mice grafted with E0771 cancer cells.

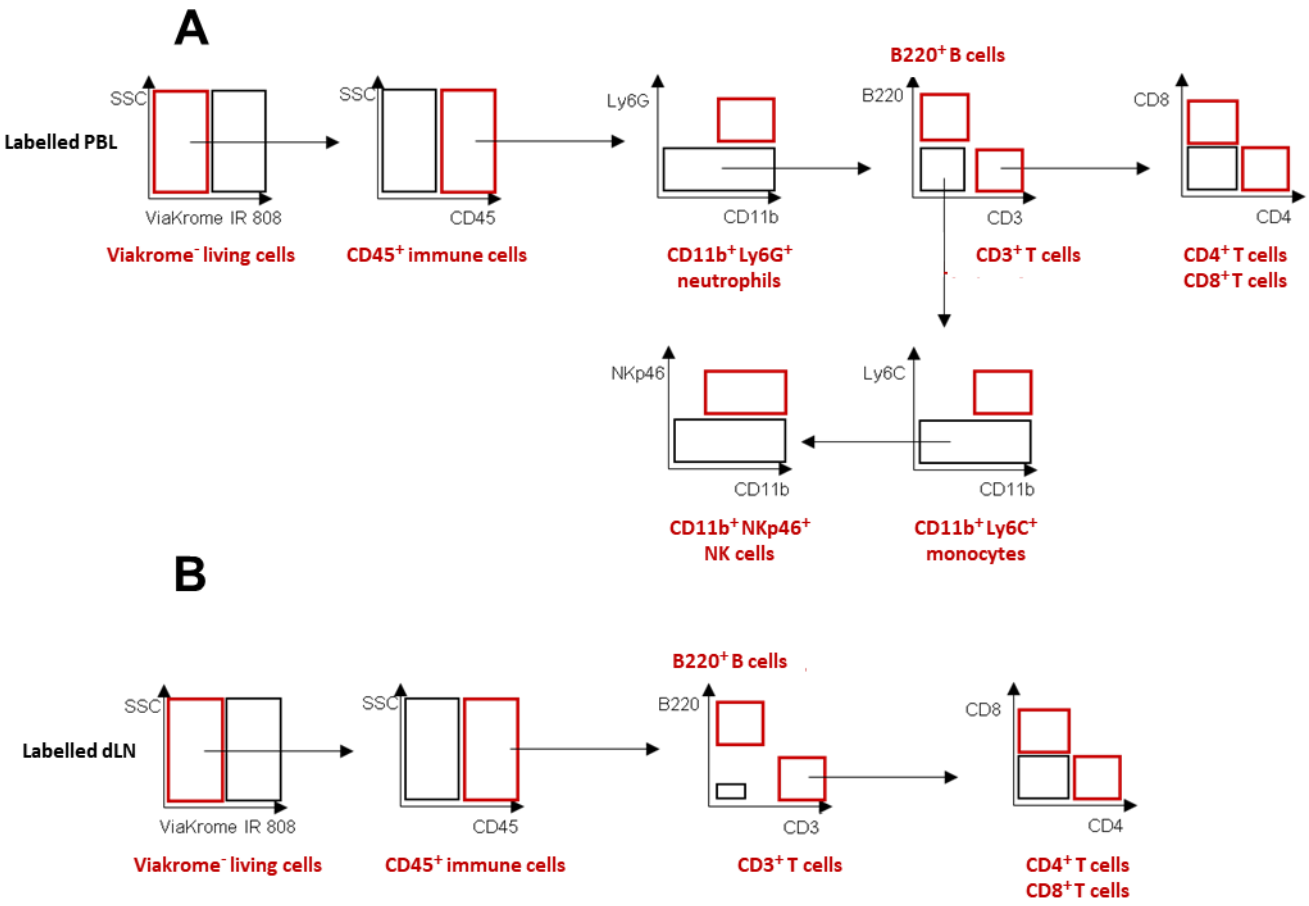

Figure S9. Schematic representation of the gating procedure to isolate immune populations in PBLs (A) and in dLNs (B) from mice grafted with TUBO cancer cells.

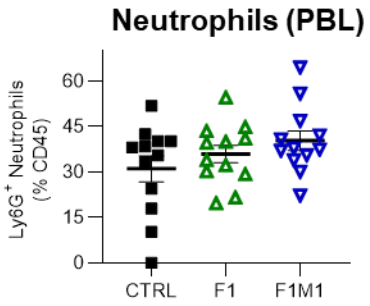

Figure S10. Anti-CathD antibody-based therapy does not affect the proportion of neutrophils in PBLs from mice grafted with TUBO cancer cells.

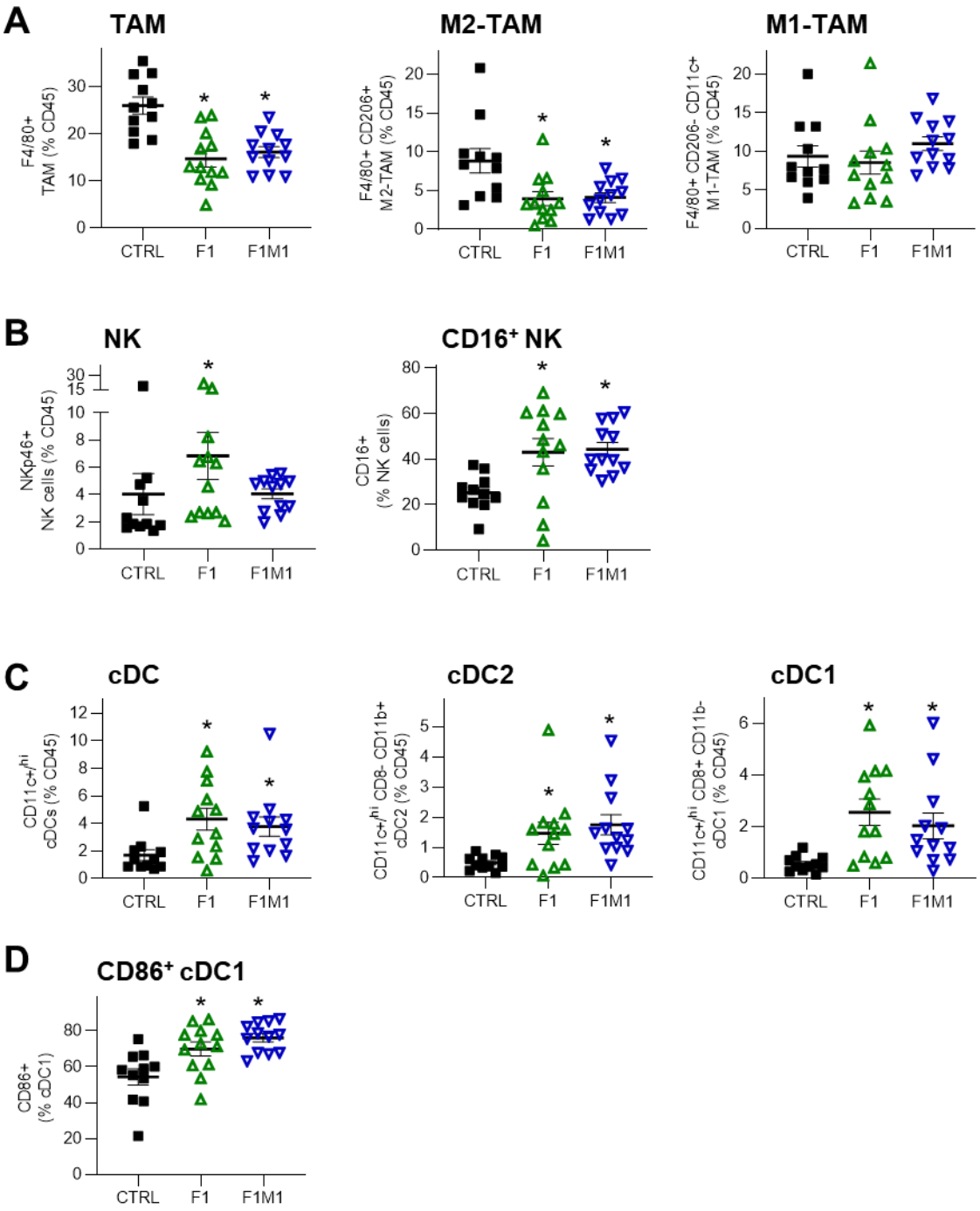

Figure S11. Anti-CathD antibody-based therapy triggers antitumor immunity in TUBO cell-derived tumors.

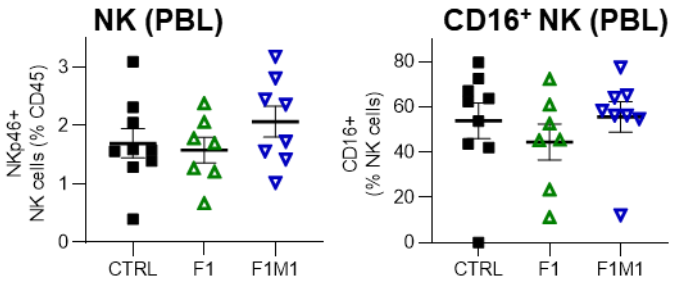

Figure S12. Anti-CathD antibody-based therapy does not affect NK cell activation in PBLs of E0771 cell-derived tumors.

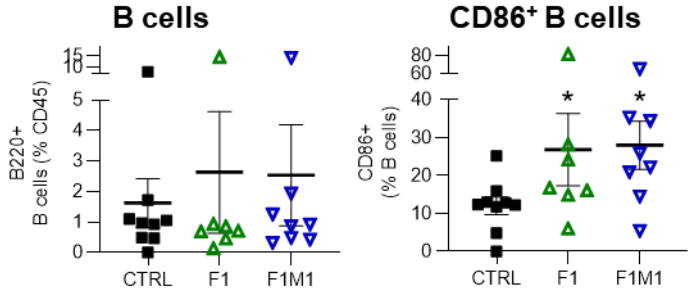

Figure S13. Anti-CathD antibody-based therapy increases the percentage of CD86+ antigen-presenting B cells in E0771 cell-derived tumors.

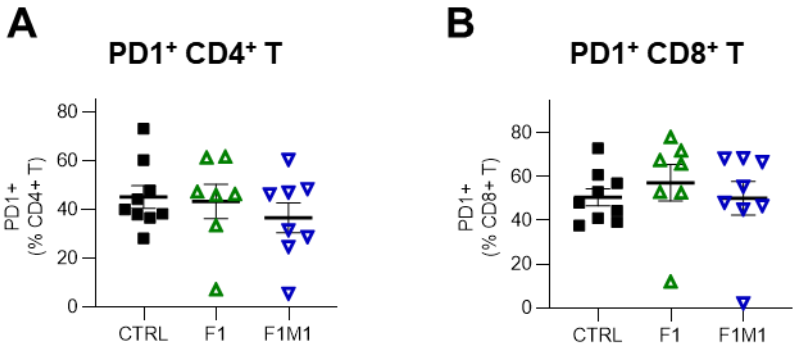

Figure S14. Effect of anti-CathD antibody-based therapy on PD-1+ T cell recruitment in E0771 cell-derived tumors.

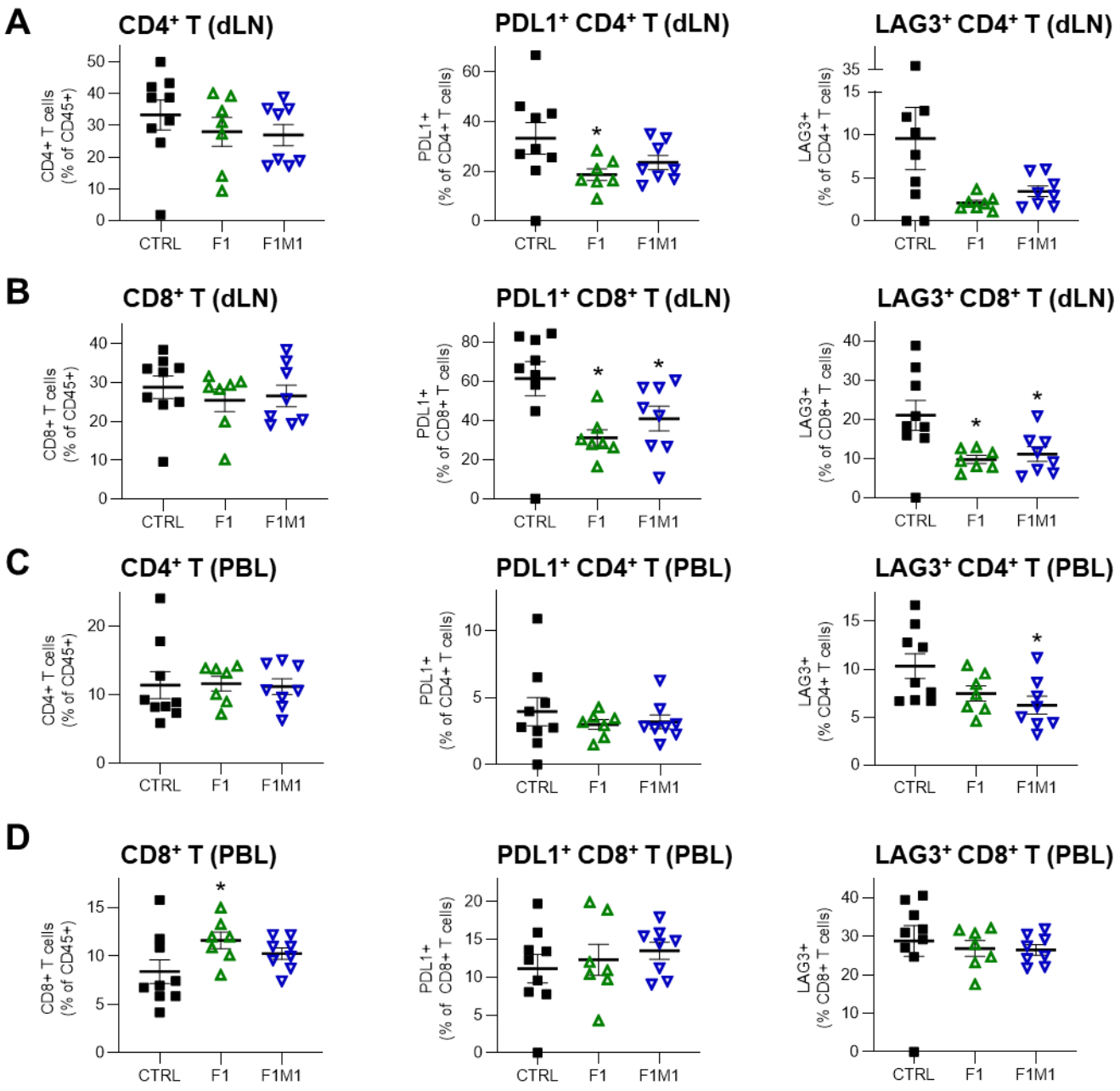

Figure S15. Anti-CathD antibody-based therapy reduces T-cell exhaustion in dLNs but not in PBLs from mice grafted with E0771 TNBC cells.

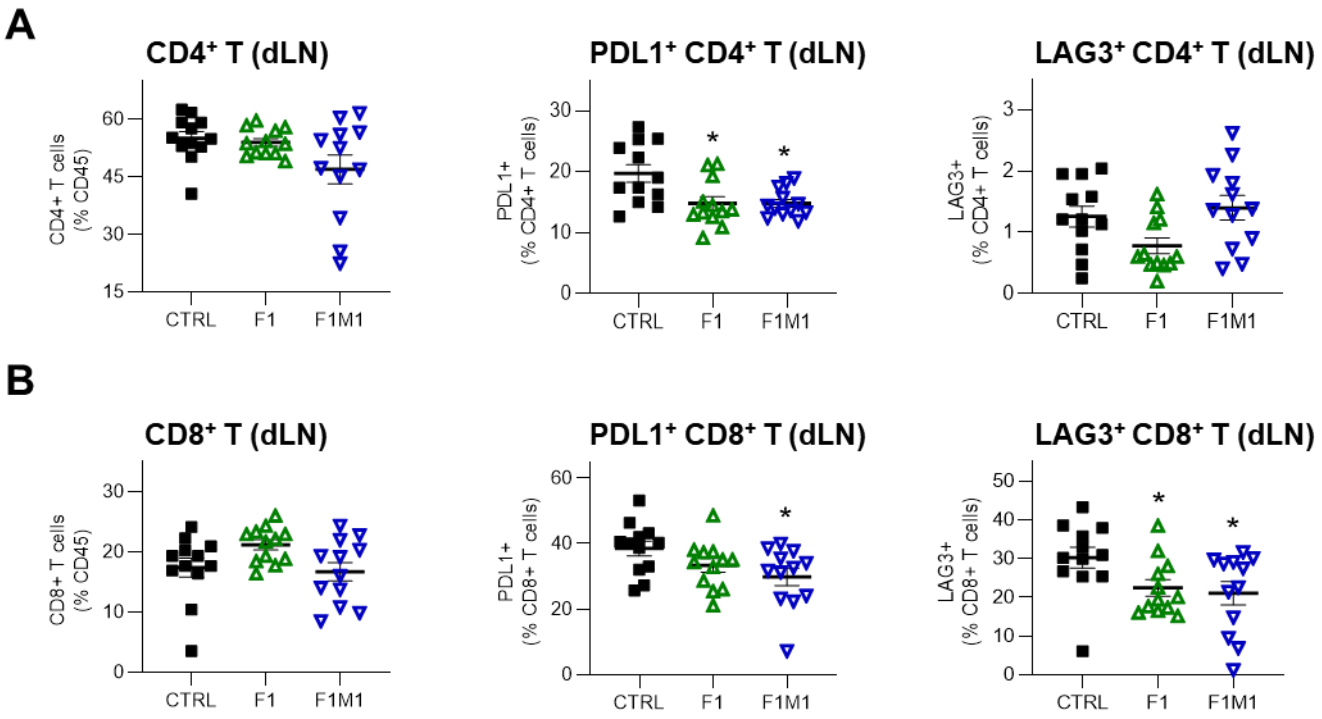

Figure S16. Anti-CathD antibody-based therapy reduces T-cell exhaustion in dLNs from mice grafted with TUBO cancer cells.

Name	Forward (5’ -> 3’)	Reverse (5’ -> 3’)
B2m	ATGGCTCGCTCGGTGACCCT	TTCTCCGGTGGGTGGCGTGA
Ccl2	TTAAAAACCTGGATCGGAACCAA	GCATTAGCTTCAGATTTACGGGT
Ccr2	GGAAGACAATAATATGTTACCTCAGTTCA	GTGTGGTGGCCCCTTCATC
Fcgr1	AGGTTCCTCAATGCCAAGTG	ATTCTTCCATCCGTGACACC
Fcgr2b	CTAGGAAGGACACTGCACCA	GACAGCAATCCCAGTGACAG
Fcgr3	AATGCACACTCTGGAAGCCAA	CACTCTGCCTGTCTGCAAAAG
Fcgr4	ATGTGGCAGCTACTACTACCA	ACCCACTTGGGGTCTAGGTTC
Fcgrt	CATTGCTGGAGGTCAAACGTGG	CGATTCCAACCACAGGCACAGA
Foxp3	GGCCCTTCTCCAGGACAGA	GCTGATCATGGCTGGGTTGT
H2b1	GCTGGTGAAGCAGAGAGACTCAG	GGTGACTTTATCTTCAGGTCTGCT
H2d1	AGTGGTGCTGCAGAGCATTACAA	GGTGACTTCACCTTTAGATCTGGG
Il4	ATCCTGCTCTTCTTTCTCGAATGT	GCCGATGATCTCTCTCAAGTGATT
Il10	CAGCCGGGAAGACAATAACTG	CCGCAGCTCTAGGAGCATGT
Il12p40	GGTGCAAAGAAACATGGACTTG	GACAGAGACGCCATTCCACAT
Il15	ACAGAGGCCAACTGGATAGATG	TGCAATTCCAGGAGAAAGCA
Rps9	CGGCCCGGGAGCTGTTGACG	CTGCTTGCGGACCCTAATGTGAC
Tigit	GTCTTCAGTGATCGGGTGGT	GCCACTGAGCTTTCTTGGAC
Tnf	CTGAACTTCGGGGTGATCGG	GGCTTGTCACTCGAATTTTGAG

Table S1. Sequences of the primers used for RT-qPCR.